Coordination Chemistry Reviews 253 (2009) 2244–2260

Contents lists available at ScienceDirect

Coordination Chemistry Reviews

journal homepage: www.elsevier.com/locate/ccr

Review

Coordination chemistry of Robson-type polyamine-dithiophenolate macrocycles: Syntheses, structures and magnetic properties of dinuclear complexes of first-row transition metals

Vasile Lozan[a], Claudia Loose[b], Jens Kortus[b,*], Berthold Kersting[a,**]

[a] Fakultät für Chemie und Mineralogie, Universität Leipzig, 04103 Leipzig, Germany
[b] Fakultät für Chemie und Physik, TU Bergakademie Freiberg, 09599 Freiberg, Germany

Contents

ARTICLE INFO

Article history:
Received 4 July 2008
Accepted 31 August 2008
Available online 9 September 2008

Keywords:
Binucleating amine-thiophenolate ligands
N-functionalization
Coordination chemistry
Structures
Magnetic properties

ABSTRACT

The coordination chemistry of N-functionalized derivatives of Robson-type macrocyclic hexamine-dithiophenolate ligands $(L^R)^{2-}$ is presented in this review. The ligands form mononuclear as well as dinuclear transition metal complexes of first row-transition metal ions. The bioctahedral transition metal complexes of the type $[M_2(L^R)(\mu\text{-}L')]^+$ exhibit a rich coordination chemistry since the active coordination site L′ is accessible for a wide range of exogenous coligands. It is demonstrated that N-functionalization of the secondary NH groups influences many properties of the binuclear $[M^{II}_2(L^R)(\mu\text{-}L')]^+$ complexes, including color, molecular and electronic structure, hydrogen bonding interactions, redox potential, complex stability, and reactivity. The magnetic exchange interactions in these complexes both from an experimental as well as a theoretical point of view are also a subject of this article.

1. Introduction

In recent years much effort has been put in synthesis and characterization of mono- and poly-nuclear transition-metal thiolate complexes [1–6]. The pronounced interest in these compounds is primarily due to both their biological relevance as simple model compounds for the active sites of metalloenzymes [7–10] and their intriguing magnetic and electronic properties [11–13]. Macrocyclic

* Corresponding author. Tel.: +49 3731 39 4008; fax: +49 3731 39 4005.
** Corresponding author. Tel.: +49 341 973 6143; fax: +49 341 973 6199.
E-mail addresses: Jens.Kortus@physik.tu-freiberg.de (J. Kortus), b.kersting@uni-leipzig.de (B. Kersting).

0010-8545/$ – see front matter © 2008 Elsevier B.V. All rights reserved.
doi:10.1016/j.ccr.2008.08.016

ligands are particularly suited for the synthesis of such complexes as they are more stable than their acyclic counterparts and the two metal ions are fixed in close proximity which has important implications for the metal–metal interactions [14] and the binuclear metal reactivity [15–17]. In the past most of the pertinent studies had focused on binucleating phenolate-based ligands and it is only recently that the coordination chemistry of the corresponding thiophenolate-based macrocycles has been investigated [18]. The aim of this review is to highlight certain aspects concerning the synthesis, structures and magnetic properties of such complexes.

2. Binucleating thiophenolate macrocycles

One of the most efficient syntheses of macrobinucleating ligands such as the tetraimine-diphenol H_2L^1 (Fig. 1) involves a Schiff base condensation of 2,6-diformyl-4-methyl-phenol with an aliphatic α,ω-diamine in the presence of a labile first-row transition metal ion. This elegant one-step method provides the ligands in good to excellent yield as their dinuclear metal(II) complexes $[M_2LX_2]$ (X = anion). Since its discovery by Robson and co-worker in 1970 [19], this reaction has been successfully applied to a large number of other phenolate-based Schiff bases. The reader is directed to earlier reviews on macrobicyclic polyaza-phenolate ligands for excellent introductions to this area [20–23]. The synthesis of the free Schiff bases has been described by Schröder et al. [24] and more recently by Ustynyuk and co-workers [25].

2.1. Thiophenolate Schiff-base macrocycles

The synthesis of macrocyclic ligands incorporating thiolate donors has also been actively pursued within the past several years, motivated primarily by their ability to model the active site of dinuclear metalloenzymes [26–28]. An early example incorporating alkyl thiols is the hexadentate N_4S_2 ligand H_2L^2 (Fig. 2) derived from the condensation of bis(1,5-diamine-pentane-3-thiolato)dinickel(II) with formaldehyde and nitroethane in aqueous basic solution [29].

In 1993, Schröder and co-workers reported the synthesis of a dinuclear nickel complex of the first thiophenolate Schiff-base macrocyclic complex $[Ni_2(L^3)](PF_6)_2$ [30] (Fig. 2). The complex was obtained in low yields by reaction of $[Ni(OAc)_2]\cdot 4H_2O$ with 2,6-diformyl-4-methyl-thiophenol and 1,3-diaminopropane in acetonitrile. Concurrently, Brooker et al. had independently developed a robust synthesis of H_2L^3 and this was subsequently detailed in the literature [31]. This approach makes use of the protected thiophenolate precursor *S*-(2,6-diformyl-4-methylphenyl)dimethylthiocarbamate, whose masking $CO(NMe_2)$ group is readily removed in situ by base hydrolysis. Since then this protocol has been used in the metal-directed template synthesis of several other macrobinucleating thiophenolate Schiff-base ligands [32–42] but, to date, no free thiophenols of this sort have been reported. The work incorporating the synthesis of the (2 + 2) thiophenolate Schiff-base macrocyclic complexes can be found in recent reviews by Brooker [18], Schröder [24] and Tamburini and co-workers [43] and will therefore not be discussed further here. This review will focus specifically on the synthesis and coordination chemistry of binucleating polyamine-dithiophenolate ligands, the reduced versions of thiophenolate-based Schiff-bases.

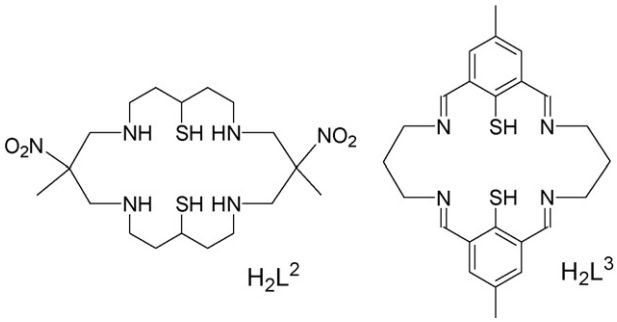

Fig. 2. Structure of macrobinucleating ligands H_2L^2 [29] and H_2L^3 [30].

2.2. Polyamine-dithiophenolate macrocycles

The reduction of the imine donors is expected to affect the ligating properties of the Schiff-base thiophenolate ligands significantly due to a significantly decreased ligand field strength and the sterically more demanding (sp^3-hybridized) amine functions of the resulting polyamine-dithiophenolates [44]. In addition, such macrocycles should be hydrolytically more robust than their parent Schiff bases [45–48]. Brooker and co-workers described the first such complex, $[Ni_2(L^4)](ClO_4)_2$, in 1998 (Fig. 3). The complex $[Ni_2(L^4)](ClO_4)_2$ was prepared in good yields by the reduction of $[Ni_2(L^3)](ClO_4)_2$ with $NaBH_4$ in MeOH followed by acidic workup [36].

The 24-membered Robson-type hexaaza-dithiophenolate ligand H_2L^5 and its various derivatives have been utilized by Kersting and co-workers as supporting ligands for dinuclear complexes with a bioctahedral $N_3M(\mu\text{-}S_2)_2(L')MN_3$ core structure (Scheme 1). The macrocycle H_2L^5 was prepared by a [1 + 2] condensation reaction of the tetraaldehyde **1** with 2 equiv. of diethylenetriamine in $EtOH/CH_2Cl_2$ using medium-dilution conditions followed by two successive reductions with $NaBH_4$ and Na/NH_3 [49,50]. The yield of the macrobicycle **2a** is excellent (>90%), attributable to the template

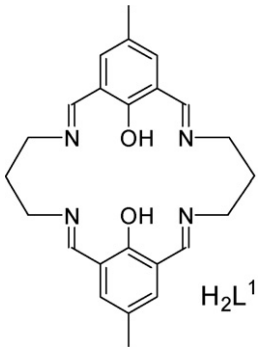

Fig. 1. Structure of the macrobinucleating ligand H_2L^1 [19].

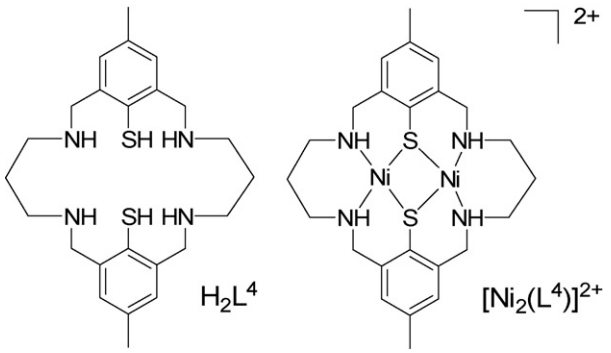

Fig. 3. Structure of H_2L^4 and its dinickel(II) complex [36].

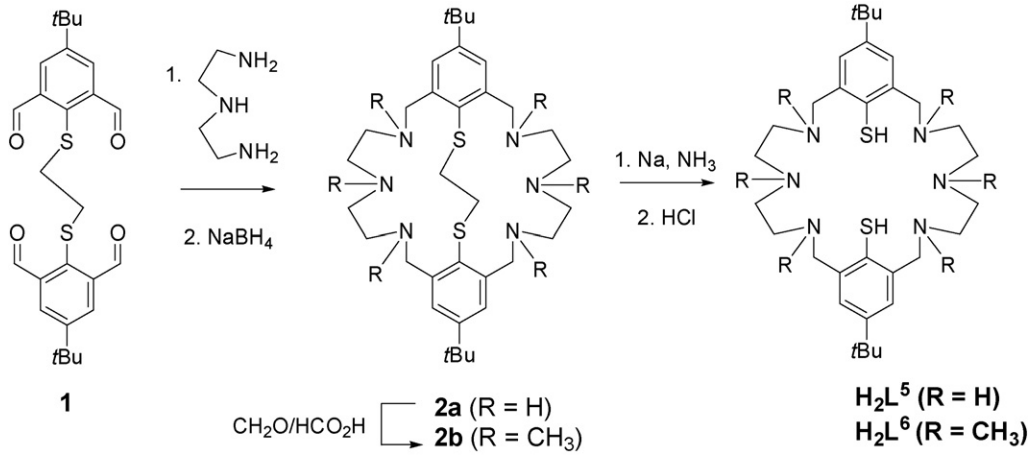

Scheme 1. Synthesis of H_2L^5 and H_2L^6 [49,50].

effect of the bridging ethylene unit which predisposes the four aldehyde groups during the Schiff-base formation step [51–53]. Similar reactions of **1** with ethylenediamine or propylenediamine yielded tricyclic [2+4] macrocycles because these diamines cannot easily span the aldehyde functions of **1** [54,55].

An attractive feature of the macrobicyclic intermediate **2a** compared to unprotected thiolate ligands is that its secondary amines are readily alkylated without affecting the masked thiolate functions [56]. Thus, reductive methylation of **2a** with formaldehyde and formic acid under Eschweiler–Clarke conditions, followed by deprotection of **2b** with Na/NH_3 provides the permethylated derivative H_2L^6 in nearly quantitative yield. Several other aza-thioethers **2c-p** and their corresponding thiolate ligands were prepared by this route (see Fig. 4 and Table 1) and some of them will be further discussed in later sections [57–62].

The molecular structures of the macrobicycles **2b** [63], **2h** [59], and **2k** [58] have been determined by X-ray crystallography. Fig. 5 displays the structure of **2h**. The aza-thioether adopts a highly folded conformation, which is reminiscent of calixarenes [64] and related Schiff-base macrocycles [24].

The aza-thioethers **2a**,**b** can also be deprotected in similar good yields with Li/naphthalene in THF [61]. Cleavage of the thioether functions of **2b** commenced also with $[PdCl_2(NCMe)_2]$ but only partially [63] (Scheme 2). The crystal structure of the reaction product, $[Pd_2(L^{6\prime})]Cl$ (**3·Cl**), reveals two distorted-square planar PdN_2ClS units which are bridged by the thiophenolate donor of $(L^{6\prime})^-$. The vinyl-thioether moiety and the two remaining amine donors of $(L^{6\prime})^-$ do not interact with the two palladium ions.

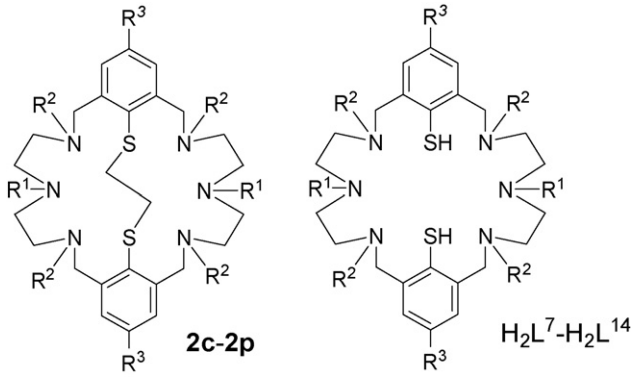

Fig. 4. Binucleating aza-thioethers **2c**–**2p** and amine-thiophenolate macrocycles H_2L^7–H_2L^{14} (see Table 1 for ligand designations) [57–62].

Table 1
Binucleating aza-thioethers **2c**–**2o** and amine-thiophenolates H_2L^7–H_2L^{14}

	R^1	R^2	R^3	[Ref]
2c	H	H	H	[62]
2d	H	H	Ph	[59]
2e	H	H	4-*t*Bu-Ph	[59]
2f	CH_3	CH_3	H	[62]
2g	CH_3	CH_3	Ph	[59]
2h	CH_3	CH_3	4-*t*Bu-Ph	[59]
2i	C_2H_5	C_2H_5	*t*Bu	[57]
2j	nC_3H_7	nC_3H_7	*t*Bu	[57]
2k	CH_3	C_2H_5	*t*Bu	[58]
2l	CH_3	H	*t*Bu	[58]
2m	$(CH_2)_2OMe$	$(CH_2)_2OMe$	*t*Bu	[61]
2n	$(CH_2)_2OH$	$(CH_2)_2OH$	*t*Bu	[61]
2o	$(CH_2)_3NH_2$	$(CH_2)_3NH_2$	*t*Bu	[61]
2p	$(CH_2)_2CN$	$(CH_2)_2CN$	*t*Bu	[61]
H_2L^7	CH_3	CH_3	H	[62]
H_2L^8	C_2H_5	C_2H_5	*t*Bu	[57]
H_2L^9	nC_3H_7	nC_3H_7	*t*Bu	[57]
H_2L^{10}	CH_3	C_2H_5	*t*Bu	[58]
H_2L^{11}	CH_3	H	*t*Bu	[58]
H_2L^{12}	$(CH_2)_2OMe$	$(CH_2)_2OMe$	*t*Bu	[61]
H_2L^{13}	$(CH_2)_2OH$	$(CH_2)_2OH$	*t*Bu	[61]
H_2L^{14}	$(CH_2)_3NH_2$	$(CH_2)_3NH_2$	*t*Bu	[61]

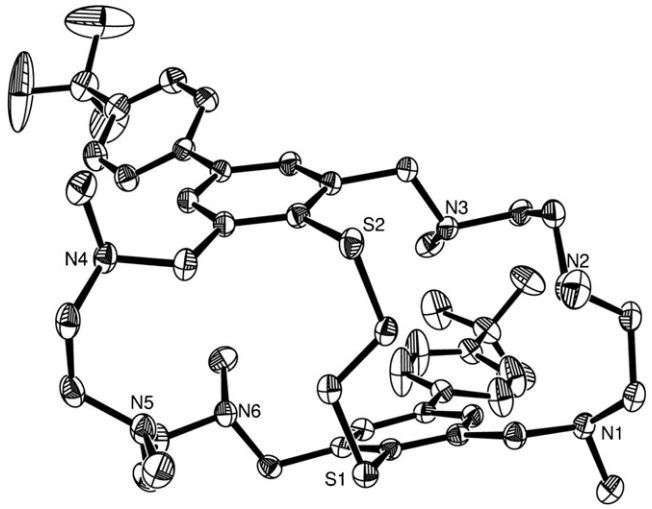

Fig. 5. Molecular structure of **2h** in the crystal. This figure was generated using data downloaded from The Cambridge Crystallographic Data Centre (CCDC) and corresponds to a structure originally reported in Ref. [59].

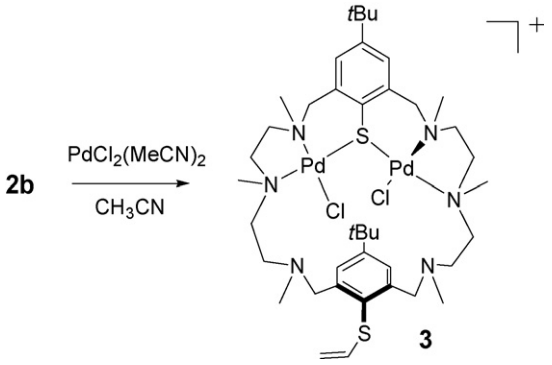

Scheme 2. Synthesis of **3** [63].

3. Coordination chemistry of polyamine-dithiophenolate macrocycles

The present review is mainly concerned with the coordination chemistry of the polyamine-dithiophenolate macrocycles H_2L^5 and H_2L^6. A large number of mono- and di-nuclear metal complexes of the deprotonated ligands have been reported within the past 10 years. In the following, selected examples originating from this work will be presented and discussed.

3.1. Mononuclear complexes

Mononuclear complexes of dinucleating macrocyclic ligands represent versatile starting materials for the preparation of heterodinuclear complexes [21–23,65–67]. The vast majority of such complexes are derived from phenolate-based Schiff bases such as H_2L^1 and its various derivatives [68–72].

Recently, Kersting and co-workers have described the first examples of mononuclear complexes of the hexaamine-dithiophenolate ligands H_2L^6 and H_2L^9 [73]. The complexes $[Ni(H_2L^6)]^{2+}$ (**6**), $[Zn(H_2L^6)]^{2+}$ (**7**), and $[Ni(H_2L^9)]^{2+}$ (**8**) (Fig. 6) were obtained by stoichiometric complexation reactions of the free ligands with the corresponding metal dichlorides and NEt_3 in methanolic solution. In the crystal, the divalent metal ions assume distorted square-pyramidal N_3S_2 coordination environments, with the τ-values ranging from 0.01 to 0.41 [74]. The two hydrogen atoms attached to the non-coordinating benzylic amine functions are hydrogen bonded to the metal-bound thiophenolate groups. A comparison with the structures of analogous complexes **4** and **5** of the acyclic ligands H_2L^{15} and H_2L^{16}, respectively, shows that the macrocycles do not confer unusual coordination geometries on the metal ions.

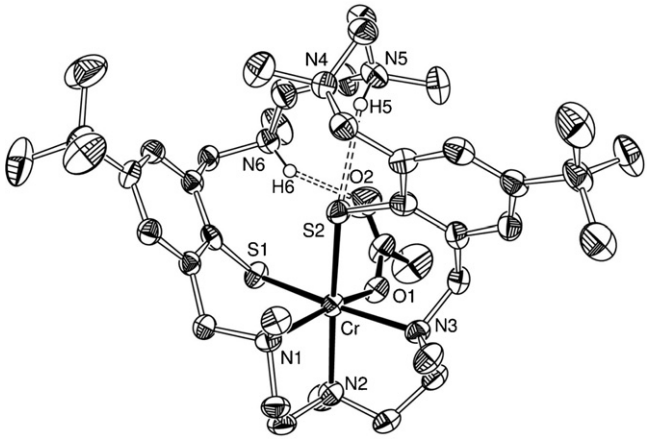

Fig. 7. Molecular structure of **9**. This figure was generated using data downloaded from The Cambridge Crystallographic Data Centre (CCDC) and corresponds to a structure originally reported in Ref. [75].

The reaction of $(L^6)^{2-}$ with $CrCl_2$ and NaOAc followed by air-oxidation produced the mononuclear complex $[Cr^{III}(H_2L^6)(OAc)]^{2+}$ (**9**) [75] (Fig. 7). The Cr^{III} ion is bonded to three N and two S atoms of $(L^6)^{2-}$ and an O atom of a monodentate acetate coligand. To our knowledge, mononuclear complexes of macrocyclic thiophenolate Schiff bases have not been documented previously in the literature [76].

3.2. Dinuclear complexes: complex types and ligand conformations

The ligands H_2L^5–H_2L^{14} are effective dinucleating ligands towards various divalent metal ions. Complexes of composition

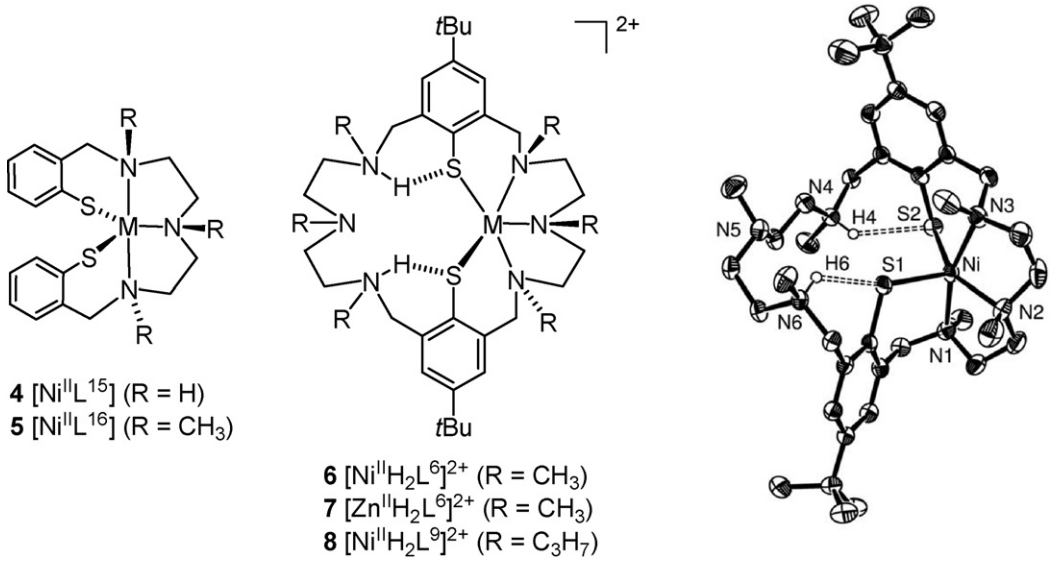

Fig. 6. (Left) Mononuclear Ni(II) and Zn(II) complexes of acyclic and macrocyclic polyamine-thiophenolate ligands. (Right) Molecular structure of **6** in the crystal. This figure was generated using data downloaded from The Cambridge Crystallographic Data Centre (CCDC) and corresponds to a structure originally reported in Ref. [73].

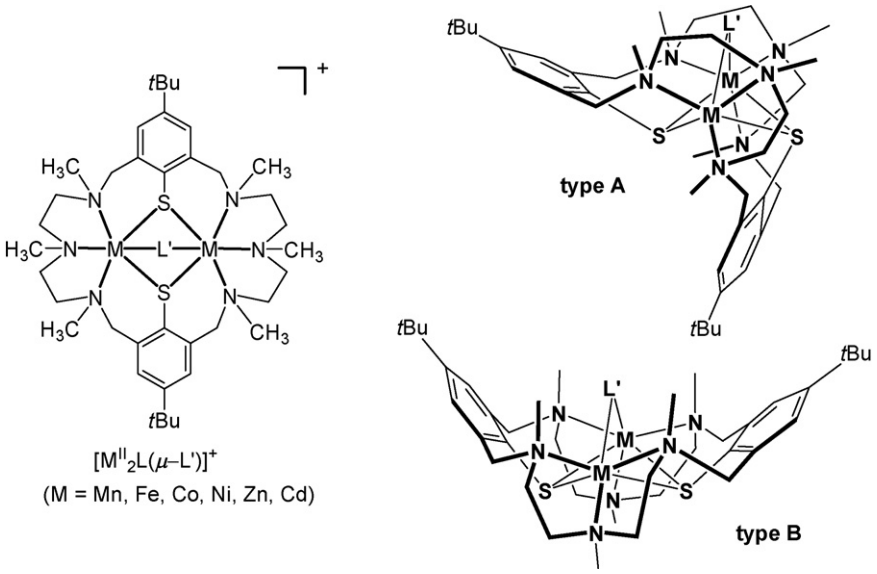

Fig. 8. Cationic $[M^{II}_2(L^R)(\mu\text{-}L')]^+$ complexes supported by the ligands $(L^R)^{2-}$ and schematic representation of their structures (L′ = coligand) [56,77].

$[M^{II}_2(L^R)(\mu\text{-}L')]^+$ (M = Mn, Fe, Co, Ni, Zn, Cd) bearing Cl^- and OAc^- coligands (L′) (Fig. 8) can be readily obtained by treatment of the free ligands H_2L^R with two equivalents of the corresponding metal(II) dihalogenides (MCl_2) or acetates ($M(OAc)_2$) in methanolic solution in the presence of a base. Table 2 lists a selection of the synthesized complexes and their labels.

All cations **10**–**29** feature a bioctahedral $N_3M(\mu\text{-}S)_2(\mu\text{-}L')MN_3$ core structure, irrespective of the type of the coligand or supporting ligand. Fig. 9 illustrates the molecular structures of the bioctahedral nickel complexes **14** and **16**, which are representative for all complexes. The divalent metal ions are coordinated in a square-pyramidal fashion by the two *fac*-$N_3(\mu\text{-}S)_2$ donor sets of the macrocycles. Upon coordination of the exogenous coligands (L′) distorted octahedral environments result for the metal atoms. The M···M distances vary from 3.037 to 3.512 Å.

Table 2
Synthesized complexes, their labels, and structure types[a]

Complex		Structure	[d(M···M)/Å]	Refs.
10	$[Ni_2(L^6)(\mu\text{-}OAc)]^+$	B	3.483(1)	[77]
11	$[Zn_2(L^6)(\mu\text{-}OAc)]^+$	B	3.427(1)	[77]
12	$[Cd_2(L^6)(\mu\text{-}OAc)]^+$	B	3.402(2)	[78]
13	$[ZnCd(L^6)(\mu\text{-}OAc)]^+$	B	n.d.[b]	[73]
14	$[Ni_2(L^5)(\mu\text{-}Cl)]^+$	A	3.098(2)	[56]
15	$[Co_2(L^5)(\mu\text{-}Cl)]^+$	n.d.[b]		[49]
16	$[Ni_2(L^6)(\mu\text{-}Cl)]^+$	A	3.184(1) [3.217(2)][c]	[56]
17	$[Co_2(L^6)(\mu\text{-}Cl)]^+$	A	3.165(1) [3.194(1)][c]	[77]
18	$[Ni_2(L^{11})(\mu\text{-}Cl)]^+$	A	3.074(1)	[58]
19	$[Cd_2(L^5)(\mu\text{-}Cl)]^+$	A	3.267(2)	[58]
20	$[Cd_2(L^6)(\mu\text{-}Cl)]^+$	B	3.3584(9)	[58]
21	$[Cd_2(L^{11})(\mu\text{-}Cl)]^+$	A	3.267(1)	[58]
22	$[Cd_2(L^{10})(\mu\text{-}Cl)]^+$	B	3.3550(8) [3.3387(8)][c]	[58]
23	$[Mn_2(L^6)(\mu\text{-}OAc)]^+$	B	3.456(1)	[75]
24	$[Fe_2(L^6)(\mu\text{-}OAc)]^+$	B	3.421(1)	[75]
25	$[Co_2(L^6)(\mu\text{-}OAc)]^+$	B	3.448(1)	[79]
26	$[Co_2(L^8)(\mu\text{-}OAc)]^+$	B	3.482(1)	[57]
27	$[Zn_2(L^8)(\mu\text{-}OAc)]^+$	B	3.460(1)	[57]
28	$[Ni_2(L^9)(\mu\text{-}OAc)]^+$	B	3.512(1)	[57]
29	$[Ni_2(L^6)(\mu\text{-}OH)]^+$	A	3.037(3)	[56]

[a] The complexes were isolated as ClO_4^- or BPh_4^- salts.
[b] Not determined.
[c] There are two independent molecules in the unit cell. The values in square brackets correspond to the second molecule.

Interestingly, the macrocycles can adopt two different conformations A and B (Fig. 8), which are reminiscent of the "partial cone" and "cone" conformations of the calixarenes. A detailed comparison of the individual structures has shown that the conformation of the amino-thiophenolates $(L^R)^{2-}$ is coupled to the size of the coligand L′ and the metal ion radii [58,80]. For the complexes of the 3d elements the type A conformation is only seen for small monoatomic bridging ligands such as $L' = OH^-$ and Cl^-. For large monoatomic coligands (such as SH^-) or a multiatom bridging ligand (such as OAc^-) the bowl-shaped conformation B is assumed, the driving force being the more regular octahedral coordination environments about the M^{II} ions [81].

Martell and co-workers have investigated the coordination chemistry of the analogous phenolate ligand H_2L^{17} [71,82] (Fig. 10). The complexes $[Ni_2(L^{17})]Br_2$ [83], $[Ni_2(L^{17})(H_2O)_2]Br_2$ [82], $[Zn_2(L^{17})(H_2O)_2]Br_2$ [84], and $[Cu_2(L^{17})]ClBr$ [85] were prepared and structurally characterized. Despite the identical ligand backbones, only doubly-bridged $N_3M(\mu\text{-}OR)_2MN_3$ core structures are supported [86]. In addition, these compounds have flat structures in striking contrast to the bowl- or cleft-like structures of the amine-thiophenolate complexes.

Another highly significant difference is that the nickel atoms in the phenolate complexes do not bind exogeneous coligands, and remain five-coordinate. Similar differences have been noted by Brooker, who compared the coordination chemistries of analogous phenolate and thiophenolate Schiff-bases [18]. The structure differences can be traced to the different hybridizations of the phenolate-oxygen (sp^2, trigonal-planar) and the thiophenolate-sulfur atoms (sp^3, tetrahedral). The former macrocycles tend to enforce a planar $M(\mu\text{-}OR)_2M$ core structure, while the latter feature a bent $M_2(\mu\text{-}SR)_2$ structure, which can be spanned more easily by the coligands.

A different coordination behavior of the hexamine-dithiophenolate ligand H_2L^6 was observed in the case of Hg^{II} and Pb^{II}. The complexation of H_2L^6 with $Hg(OAc)_2$ and $Pb(OAc)_2$ provided dicationic $[Hg_2(L^6)]^{2+}$ (**30**) and $[Pb_2(L^6)]^{2+}$ (**31**), respectively, which were isolated as their ClO_4^- or BPh_4^- salts [78]. These compounds show no tendency to bind further coligands. The Hg(II) ions in **30** are surrounded by three nitrogen and two sulfur donor atoms of $(L^6)^{2-}$ (coordination number of Hg^{II}: 4 + 1) (Fig. 11), while the coordination environment of each lead(II)

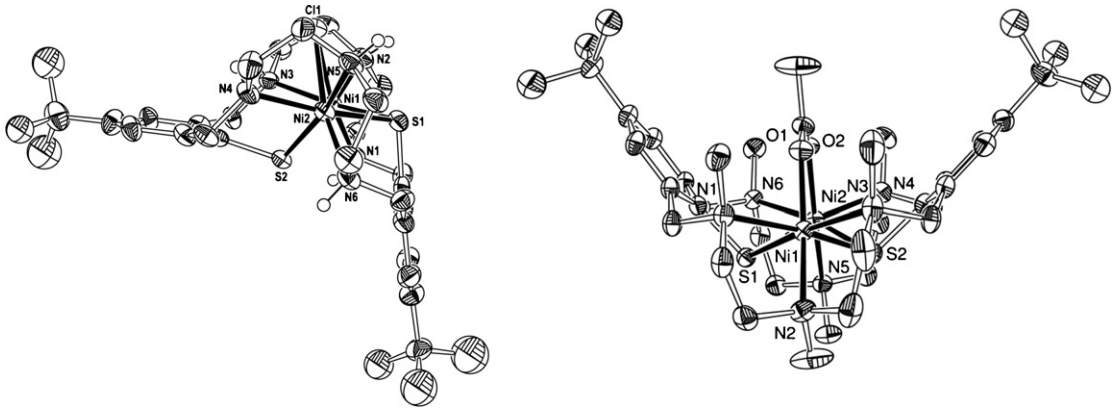

Fig. 9. Molecular structures of **14** (left) and **16** (right) in the crystal. This figure was generated using data downloaded from The Cambridge Crystallographic Data Centre (CCDC) and corresponds to the structures originally reported in Refs. [56,77].

ion in **31** consists of three amine donors and one thiophenolate sulfur atom (coordination number of Pb^{II}: 3 + 1). The coordination geometry of Pb^{II} is best considered as distorted square pyramidal, with the lead ion sitting ca 1.3 Å above the plane through the four donor atoms. The empty space above the lead(II) ion on the apex of the pyramid is indicative of a stereochemically active lone pair, like in PbO (yellow modification) [87]. These results have established also the capability of the macrobinucleating polyaza-dithiophenolate ligand to form stable binuclear complexes of toxic heavy metals.

The S-oxygenation of the hexaamine-dithiophenolate macrocycles should provide a potential entry into the novel class of binucleating polyamine-disulfonate and -disulfinate macrocycles. Indeed, such ligands can be prepared by oxidation of dinuclear nickel complexes of the parent hexaaza-dithiophenolate macrocycles followed by decomposition of the oxidation products in acidic solution. The dinuclear nickel complexes $[Ni^{II}_2(L^{18})(L')]^+$ ($L' = Cl^-$ (**32**) and OAc^- (**33**)) of the hexaaza-diphenylsulfonate ligand $(L^{18})^{2-}$ (Fig. 12) are obtained by oxidation of their respective $[Ni^{II}_2(L^6)(\mu\text{-}L)]^+$ parents ($L' = Cl^-$ (**16**), OAc^- (**10**)) with *meta*-chloroperoxybenzoic acid or hydrogen peroxide [88]. Decomposition of the sulfonate complexes gives the free macrocycle H_2L^{18}, which upon treatment with $Zn(OAc)_2{\cdot}2H_2O$ produces diamagnetic $[Zn^{II}_2(L^{18})(OAc)]^+$ (**34**). The crystal structure determination of **32** (Fig. 12) reveals a binuclear complex with bridging sulfonate and chloride groups and an overall bowl-shaped geometry.

A dinuclear Cu(II) complex of the hexaaza-disulfinate derivative $(L^{19})^{2-}$, i.e., $[Cu^{II}_2(L^{19})]^{2+}$ (**35**), forms by air-oxidation of $(L^6)^{2-}$ in the presence of Cu(I) (Fig. 13). The crystal structure determination of **35** reveals two Cu(II) ions with pseudo-square pyramidal N_3O_2 coordination spheres. The Cu···Cu distance is 4.993(1) Å.

Heterodinuclear complexes of polyamine-dithiophenolate ligands are still limited. Therefore, the ability of the mononuclear complexes **6** and **7** (see Section 3.1) to serve as starting materials for homo- and hetero-dinuclear complexes has also been examined. The reaction of **6** with $Ni(OAc)_2{\cdot}4H_2O$ proceeded smoothly and gave the homodinuclear complex $[Ni_2(L^6)(OAc)]^+$ (**10**) in almost quantitative yield (Scheme 3). Likewise, when **7** reacts with $Zn(OAc)_2{\cdot}2H_2O$ at room temperature, the dinuclear zinc complex $[Zn_2(L^6)(OAc)]^+$ (**11**) formed immediately. The reaction of **7** with $Cd(OAc)_2{\cdot}2H_2O$ in methanol produces a mixture of the heterodinuclear $[ZnCd(L^6)(OAc)]^+$ (**13**) and homodinuclear Zn_2 (**11**) and Cd_2 (**12**) complexes in a 8:1:1 ratio as indicated by ^1H NMR and ESI MS spectroscopy [73,89]. Homodinuclear **11** and **12** are also accessible

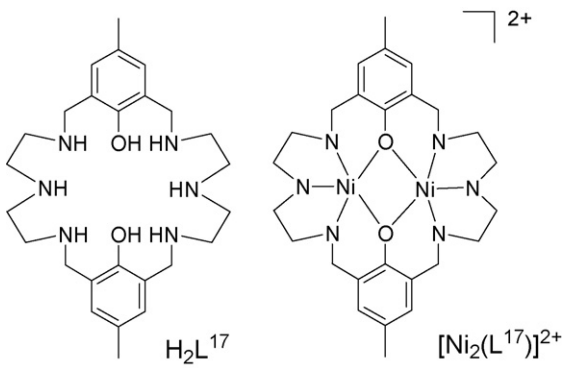

Fig. 10. Structures of the macrocycle H_2L^{17} and the $[Ni_2(L^{17})]^{2+}$ complex [83].

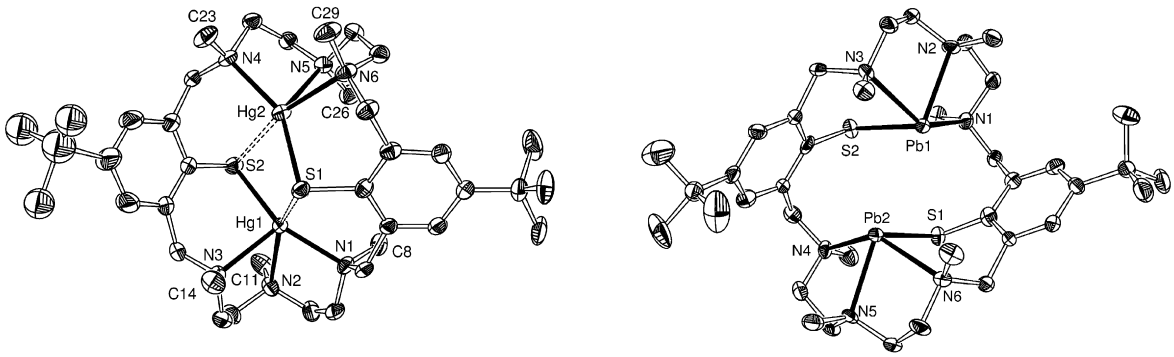

Fig. 11. Molecular structures of **30** (left) and **31** (right) in the crystal. This figure was generated using data downloaded from The Cambridge Crystallographic Data Centre (CCDC) and corresponds to the structures originally reported in Ref. [78].

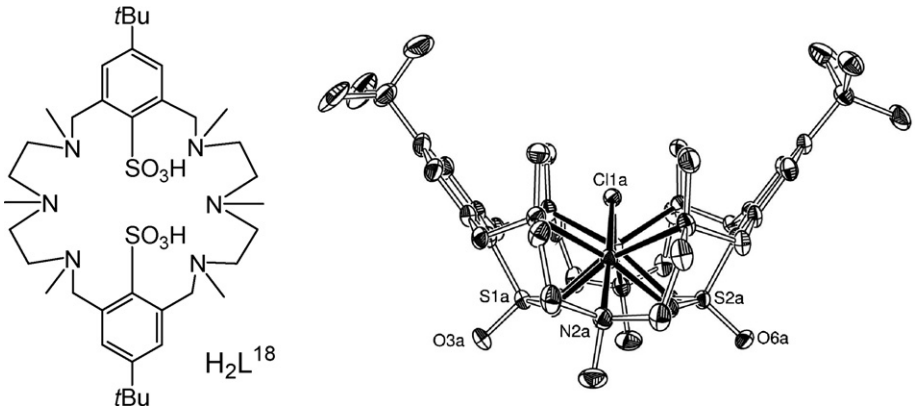

Fig. 12. (Left) Polyamine-sulfonate macrocycle H_2L^{18}. (Right) Molecular structure of **32**. This figure was generated using data downloaded from The Cambridge Crystallographic Data Centre (CCDC) and corresponds to the structure originally reported in Ref. [88].

from H_2L^6 and the corresponding metal(II) acetates. Heterodinuclear transition-metal complexes analogous to **13** would be of considerable interest, in particular with regard to their relevance to bioinorganic chemistry [90–93] and their magnetic properties [18,94–98].

3.3. Effects of N-alkylation on the molecular and electronic structures of the complexes

In the following we will focus on the properties of dinuclear transition metal complexes of the ligands H_2L^5 and H_2L^6. We also discuss only the chemistry of the 3d elements, e.g., Mn, Fe, Co, Ni and Zn. For other metal ions, see Refs. [60,78].

It is well established that the molecular and electronic structures of metal complexes of azamacrocycles are greatly affected upon N-alkylation [44]. This is mainly due to two factors: (a) the decrease of the ligand field strength and (b) the increase in the steric requirements upon going from a secondary to a tertiary amine donor function [99]. In order to examine whether the properties of the dinuclear amine-thiophenolate complexes are affected by the N-alkyl substituents, analogous complexes of the two macrocycles H_2L^5 and H_2L^6 were prepared and characterized by various spectroscopic methods (IR, UV–vis, EPR, ^{57}Fe–Mössbauer spectroscopy), cyclic voltammetry, temperature-dependent magnetic susceptibility measurements, and X-ray crystallography. The most important observations of these investigations are as follows.

- The conversion of the six secondary into tertiary amine donor functions does not change the overall structure of the $[M_2(L^R)(\mu\text{-}L')]^+$ complexes. That is the complexes retain their bioctahedral $N_3M(\mu\text{-}SR)_2(\mu\text{-}L')MN_3$ core structures and the macrocycle conformation remains constant for a given coligand, see for instance the isostructural compounds **14**–**18** [58].
- The complexes of the permethylated macrocycle H_2L^6 exhibit longer M–N and shorter M–L′ bond distances than their homologous complexes of the unfunctionalized parent H_2L^5. For instance, upon going from **14** to **16** the average Ni–N bond length increases from 2.107(6) to 2.239(2) Å (Δ = +0.132 Å) and the average N–Cl bond length decreases from 2.621 to 2.442 Å (Δ = −0.179 Å). In other words, N-alkylation of the amine-thiophenolate ligand H_2L^5 results in stronger metal–coligand bonding interactions. This in turn results in a stronger polarization of the bridging coligands and thus in a higher reactivity (Lewis-acidity) of the $[M_2(L^6)(\mu\text{-}L')]^+$ complexes [77].
- The alkylation of the secondary amine functions generates a more hydrophobic microenvironment about the active coordination site. For example, in the cations **14** and **15** the coligands and the NH functions act as hydrogen bond acceptors and donors, respectively, and are involved in inter- and intra-molecular hydrogen bonding interactions [56]. No such interactions are observed for the complexes of $(L^6)^{2-}$. This drastically alters the ease of the substitution of the bridging coligands. Thus, while the μ-Cl complex **16** reacts readily with NBu_4OH in acetonitrile to produce the

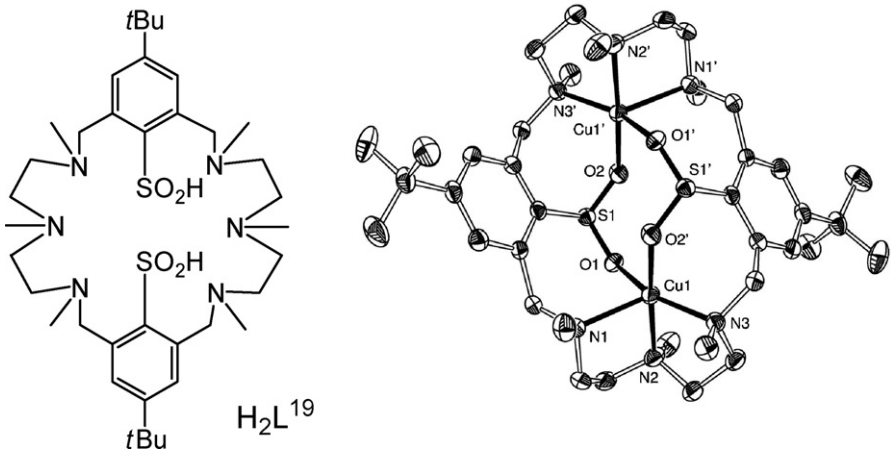

Fig. 13. (Left) Polyamine-disulfinate macrocycle H_2L^{19}. (Right) Molecular structure of **35**. This figure was generated using data downloaded from The Cambridge Crystallographic Data Centre (CCDC) and corresponds to the structure originally reported in Ref. [88].

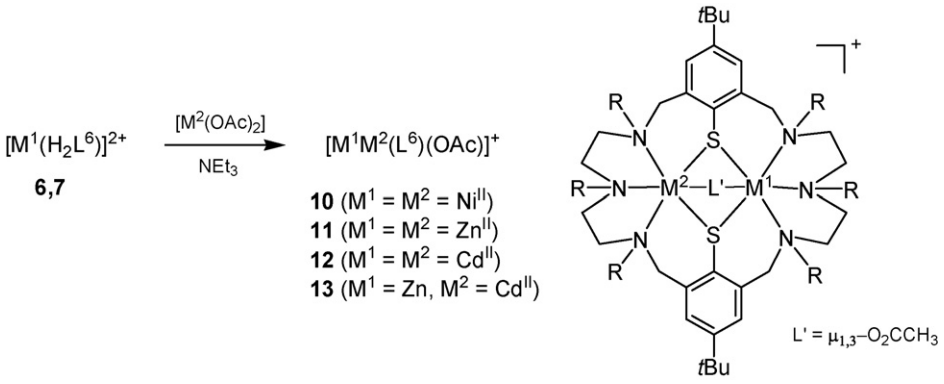

Scheme 3. Synthesis of complexes **10**–**13** [73].

hydroxo-bridged complex **29**, complex **14** was found to be unreactive [56]. Even the addition of a halide scavenger such as lead perchlorate did not lead to substitution of the Cl^- ion in **14**.

- To determine the ligand field strengths of the two macrocycles, we have analyzed the UV–vis spectra of the octahedral nickel complexes **14** and **16**. The ν_1 band ($^3A_{2g} \rightarrow {}^3T_{2g}$) in an octahedral $Ni^{II}L_6$ complex is directly related to the ligand field strength of L [100,101]. For **14**, this band is observed at 941 nm, whereas for **16** it occurs at much lower energies 1002 nm [56], showing that the donor strength of H_2L^6 is significantly weaker than H_2L^5. From the ν_1 transition one can obtain rough estimates of the octahedral splitting parameters Δ_{oct} for **14** (≈10,630 cm^{-1}) and for **16** (≈9980 cm^{-1}), respectively [101]. Such low values for Δ_{oct} (i.e., $\Delta_{oct}[Ni(H_2O)_6]^{2+} = 8500\ cm^{-1}$) are quite typical for $N_3Ni^{II}(\mu\text{-}SR)_3$ chromophores. In general, thiolates induce only weak ligand field strengths due to their poor σ-donor bonding abilities [102].
- The different ligand field strengths are also reflected in the redox potentials. Cyclic voltammetry experiments have shown that the dinickel(II) complex **14** undergoes two one-electron oxidations at +0.27 and at +1.05 V vs. SCE which correspond to the formation of the mixed-valent $Ni^{II}Ni^{III}$ and the fully oxidized $Ni^{III}Ni^{III}$ forms [56]. The cyclic voltammogram of **16** also reveals two redox waves, but this complex is oxidized at more positive potentials at +0.43 and +1.37 V vs. SCE which is in good agreement with the weaker ligand field strength of $(L^6)^{2-}$. Thus, in the $[M_2(L^6)(\mu\text{-}L')]^{n+}$ complexes the M^{III} oxidation state is enormously destabilized over the M^{II} oxidation state, even in the case of Co^{III} [79,103].
- As a consequence of the weak ligand field of $(L^6)^{2-}$, the Mn^{II}, Fe^{II}, Co^{II}, and Ni^{II} ions in the acetato-bridged complexes **23**–**25** and **10**, respectively, adopt high-spin configurations [75]. Weak intramolecular antiferromagnetic exchange interactions are present in the Mn_2^{II}, Fe_2^{II}, and Co_2^{II} complexes where $J = -5.1$, -10.6, and $-2.0\ cm^{-1}$ ($H = -2JS_1S_2$). In contrast, in the dinickel complex **10** a ferromagnetic exchange interaction is present with $J = +6.4\ cm^{-1}$. There appears to be a magneto-structural correlation between the sign of the exchange parameter J and the M–S–M bond angle. For **23**–**25** the average M–S–M angles are significantly smaller than 90° and J is negative. For **10**, however, the mean Ni–S–Ni bridging angle is very close to 90° and J has a positive value.
- Finally, the presence of the substituents on the nitrogen donors also influences the reactivity of the corresponding complexes significantly. Thus, utilization of the permethylated derivative in place of H_2L^5 drastically alters the Lewis-acidity of the metal ions, that is the coligands in the $[Ni_2(L^6)(L)]^+$ compounds become more polarized as in the $[Ni_2(L^5)(L')]^+$ complexes. Note that in the latter the Lewis-acidity of the divalent nickel(II) ions is in large part consumed for the polarization of the six secondary NH functions. This explains why only the complexes of the permethylated macrocycle are able to activate and transform small molecules such as H_2O or CO_2 [57,77,79].

In summary, the use of the permethylated derivative H_2L^6 in place of H_2L^5 influences many properties of the binuclear $[M^{II}_2(L^R)(L')]^{2+}$ complex fragments, including color, molecular and

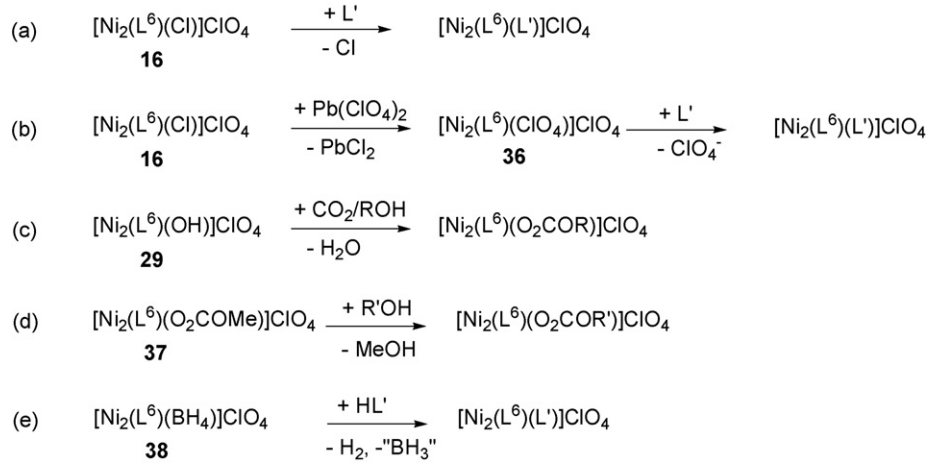

Scheme 4. Different methods used to synthesize $[Ni_2(L^6)(L')]^+$ complexes.

Table 3
Synthesized $[Ni_2(L^6)(L')]^{n+}$ complexes and their labels

	L′	Preparation method	Structure type	Coordination mode	d(M···M) (Å)	Refs.
10	$CH_3CO_2^-$	I	B	$\mu_{1,3}$	3.483(1)	[77]
29	OH^-	I	A	μ	3.037(3)	[55]
36	ClO_4^-	II	B	$\mu_{1,3}$	3.547(1)	[105]
37	$CH_3OCO_2^-$	III	B	$\mu_{1,3}$	3.491(1)	[77]
38	BH_4^-	II	B	$\mu_{1,3}$	3.458(1)	[106]
39	$EtOCO_2^-$	IV	B	$\mu_{1,3}$	3.485(1)	[77]
40	O_2CPh^-	I	B	$\mu_{1,3}$	3.470(1)	[80]
41	NO_3^-	I	B	$\mu_{1,3}$	3.492(1)	[80]
42	NO_2^-	I	B	$\mu_{1,2}$	3.398(1)	[80]
43	N_3^-	I	B	$\mu_{1,3}$	3.683(1)	[80]
44	pydz[a]	II	B	$\mu_{1,2}$	3.392(1)	[80]
45	N_2H_4	I	B	$\mu_{1,2}$	3.441(1)	[80]
46	HCO_2^-	V	B	$\mu_{1,3}$	3.480(1)	[106]
47	SH^-	V,I	B	μ	3.295(1)	[81]
48	$CpFeC_5H_4CO_2^-$	I	B	$\mu_{1,3}$	3.485(1)	[107]
49	SO_4^{2-}	I	B	$\mu_{1,3}$	3.506(1)	[105]
50	MoO_4^{2-}	I	B	$\mu_{1,3}$	n.d.	[105]
51	WO_4^{2-}	I	B	$\mu_{1,3}$	3.655(1)	[105]
52	$PhCH_2NCO_2^-$	IV	B	$\mu_{1,3}$	3.472(1)	[108]
53	HCN_4^-	I	B	$\mu_{1,2}$	3.455(1)	[109]

[a] *pydz* = pyridazine.

electronic structure, hydrogen bonding interactions, redox potential, complex stability, and ground spin-state. The reactivity is also greatly affected [104].

3.4. Variation of coligands and magnetic properties of complexes

The dinuclear amine-thiophenolate complexes have a rich coordination chemistry since their active coordination site is accessible for a large variety of neutral and charged coligands (L′). A particularly large number of dinuclear nickel(II) supported by $(L^6)^{2-}$ have been prepared.

The methods to synthesize these complexes include (Scheme 4): (a) ligand exchange using the chloro-bridged complex **16** or (b) the more substitutionally-labile perchlorato complex **36** (itself prepared by Cl^- abstraction from **16** with $Pb(ClO_4)_2$), (c) CO_2-fixation by the hydroxo-bridged complex **29**, (d) transesterification reactions using the methylcarbonato complex **37**, and (e) reduction of the boranato-bridged complex **38**. In general, these reactions were complete within a few hours at room temperature and provided the desired complexes (as their ClO_4^- or BPh_4^- salts) in good to excellent yields. A selection of the complexes prepared by these methods is listed in Table 3.

The complexes listed in Table 3, except **50**, have all been characterized by X-ray crystallography. In all cases, except **29**, the macrocycle adopts the conical-calixarene like conformation B, illustrated by two representative examples $[Ni_2(L^6)(BH_4)]^+$ (**38**) and $[Ni_2(L^6)(SH)]^+$ (**47**) (Fig. 14). The complexes are thus invariably bioctahedral with either a face-sharing or edge-sharing $N_3M(\mu\text{-}SR)_2(\mu\text{-}L')MN_3$ core structure depending on the coordination mode of the coligands. Note that the metal–metal separations (d(M···M)) correlate with the bridging mode of the coligands, i.e., $(d(\mu\text{-}L') < d(\mu_{1,2}\text{-}L') < d(\mu_{1,3}\text{-}L'))$. As is shown below, this greatly effects the magnetic exchange interactions.

Some of the complexes feature unusual ligand coordination modes. The azide complex **43** (shown in Fig. 15) is a representative example. The planarity of the Ni–N_3–Ni assembly (torsional angle $\tau = 0^\circ$) together with the remarkably obtuse Ni–N–N angles at 109.9(2)° has never been observed before for M–$\mu_{1,3}$-N_3–M linkages [110–112]. The presence of this distinct binding mode can be traced to the complementary size and form of the binding pocket of the $[Ni_2(L^6)]^{2+}$ complex. Similar effects have been observed by McKee and Nelson, who stabilized a nearly linear Ni–($\mu_{1,3}$-N_3)–Ni linkage in the cavity of a dinuclear nickel cryptate complex [113,114]. The magnetic properties of dinuclear nickel complexes with such extreme azide coordination modes are of interest, because the theory predicts unusual large intramolecular magnetic exchange interactions for such species [115,116].

The hydrazine complex **45** is an example for a complex that features an unusual conformation of a small neutral inorganic molecule. Free hydrazine exists predominantly in the *gauche* conformation at room temperature (dihedral angle $\tau \sim 100^\circ$) [117], also most commonly seen in dinuclear hydrazine complexes [118,119]. In **45** the N_2H_4 ligand can only adopt the *cis* (ecliptic) conformation ($\tau = 3.7^\circ$) (Fig. 16). To the best of our knowledge, such a

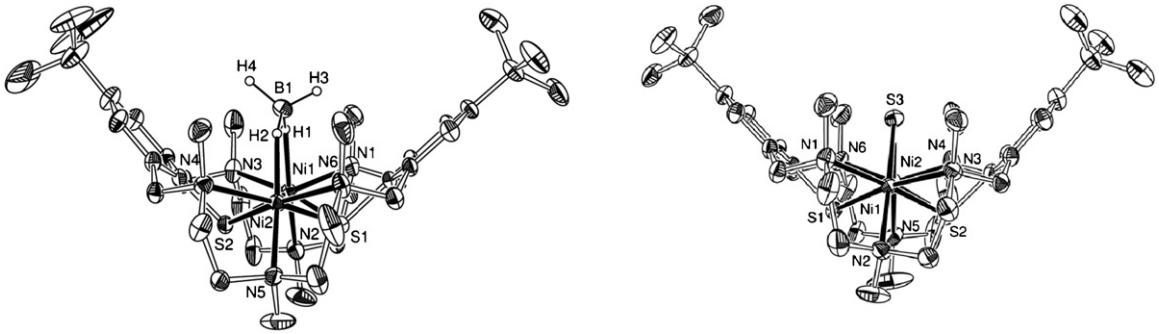

Fig. 14. Molecular structures of **38** (left) and **47** (right) in the crystal. The figures were generated using data downloaded from The Cambridge Crystallographic Data Centre (CCDC) and correspond to the structures originally reported in Refs. [81,106], respectively.

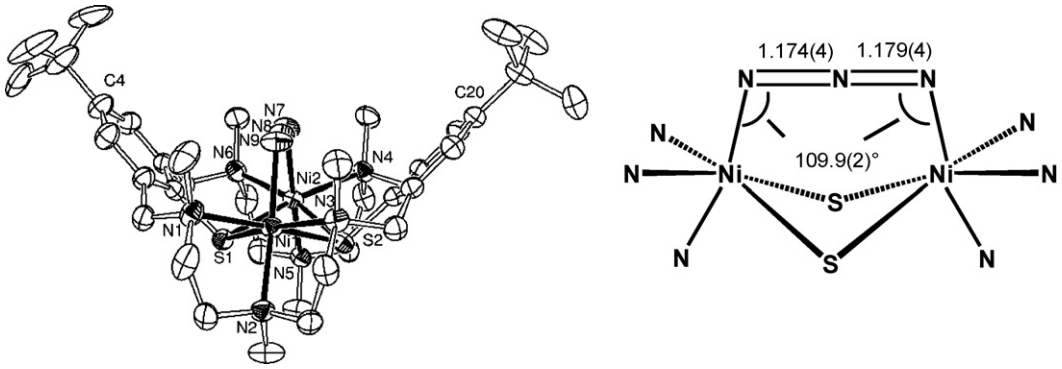

Fig. 15. (Left) Molecular structure of the cation **43** in the crystal. (Right) Central $N_3Ni(\mu\text{-}S)_2(\mu_{1,3}\text{-}N_3)NiN_3$ core in **43**. The figures were generated using data downloaded from The Cambridge Crystallographic Data Centre (CCDC) and correspond to the structure originally reported in Ref. [80].

coordination mode is without precedence in dinuclear transition metal hydrazine complexes [120–124], albeit it is documented for mononuclear species [125,126]. The ecliptic N_2H_4 conformation is presumably a consequence of repulsive $NH\cdots C_{aryl}$ van der Waals interactions between the N_2H_4 molecule and $(L^6)^{2-}$.

The temperature-dependence of the molar magnetic susceptibility of a series of dinuclear nickel complexes was examined between 2 and 300 K by using a SQUID magnetometer. Least-squares fits of the magnetic susceptibility data by full-matrix diagonalization of the appropriate spin Hamiltonian (Eq. (1)) provided the J and g values for each compound (Table 4):

$$H = -2JS_1S_2 + \sum_{i=1}^{2}\left[D_i\left(\hat{S}_{iz}^2 - \frac{1}{3}S_i(S_i+1)\right) + g_i\mu_B B_\tau \hat{S}_{i\tau}\right], \quad (\tau = x, y, z) \qquad (1)$$

All complexes, except **29** and **43**, show weak intramolecular ferromagnetic exchange interactions. The J values range from 3.5 to 27.8 cm^{-1}. An analysis of the temperature-dependent magnetic susceptibility data for **29** and **43** reveal the presence of weak antiferromagnetic exchange interactions between the Ni^{II} ions with a value for the magnetic exchange coupling constants J of −6.60 and −45.6 cm^{-1}, respectively.

The ferromagnetic exchange interaction in complexes **10**, **38**, **40**, **42**, **44**, **49** and **50** can be rationalized in terms of the Goodenough–Kanamori rules for superexchange [128]. For face-sharing bioctahedral nickel complexes a ferromagnetic exchange interaction is predicted if the Ni–X–Ni bridging angle is at 90° [129]. For smaller angles, the orthogonality of the magnetic orbitals is cancelled and antiferromagnetic pathways become available to produce a change of the sign of J. An antiferromagnetic exchange interaction, for example, is observed in tris(μ-chloro)- or tris(μ-thiophenolato)-bridged complexes, where the average bridging angle is below 80° [130,131]. The other extreme is represented by the tris(μ-phenolato)-bridged complexes, which feature wider angles at 90 ± 8° and hence parallel spin alignment occurs [132]. In our case, the Ni–(μ-SR)–Ni angles are within the range where the ferromagnetic pathway is the preferred one.

For **29** and **43**, the antiferromagnetic coupling between the two Ni^{II} ($S = 1$) ions can be explained by assuming a strong antiferromagnetic exchange interaction through the azide and hydroxide bridges which overcome the ferromagnetic coupling through the thiolate-bridges. This is, for example, supported by the fact that nearly all $\mu_{1,3}$-azido-bridged Ni^{II} ions feature an antiferromagnetic exchange interaction [133]. Moreover, it has been demonstrated that the sign and magnitude of the exchange interaction in $\mu_{1,3}$-azido-bridged Nickel complexes depend on the Ni–N–N bond angles and the Ni–N_3–Ni torsional angles [134–138] The largest antiferromagnetic exchange interaction is expected for a Ni–N–N bond angle of 108° and a torsional angle $\tau = 0°$. Our observation of a strong antiferromagnetic exchange interaction in **43** in which the azide features exactly these metrical parameters is in good agreement with the reported trend. The same arguments can be used to explain why **47**, in contrast to other triply sulfur-bridged $N_3Ni^{II}(SR)_3Ni^{II}N_3$ structures whose ground states are typically of $S = 0$, reveals an $S = 2$ ground state [81]. To date a magneto-structural correlation for face-sharing bioctahedral $Ni^{II}{}_2$ complexes has not appeared in the literature.

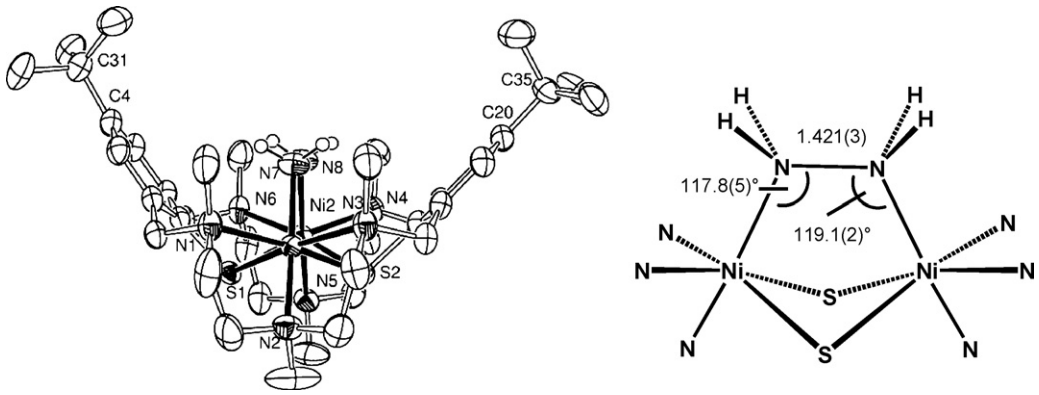

Fig. 16. Molecular structure of the hydrazine complex **45** in the crystal. The figure was generated using data downloaded from The Cambridge Crystallographic Data Centre (CCDC) and corresponds to the structure originally reported in Ref. [80].

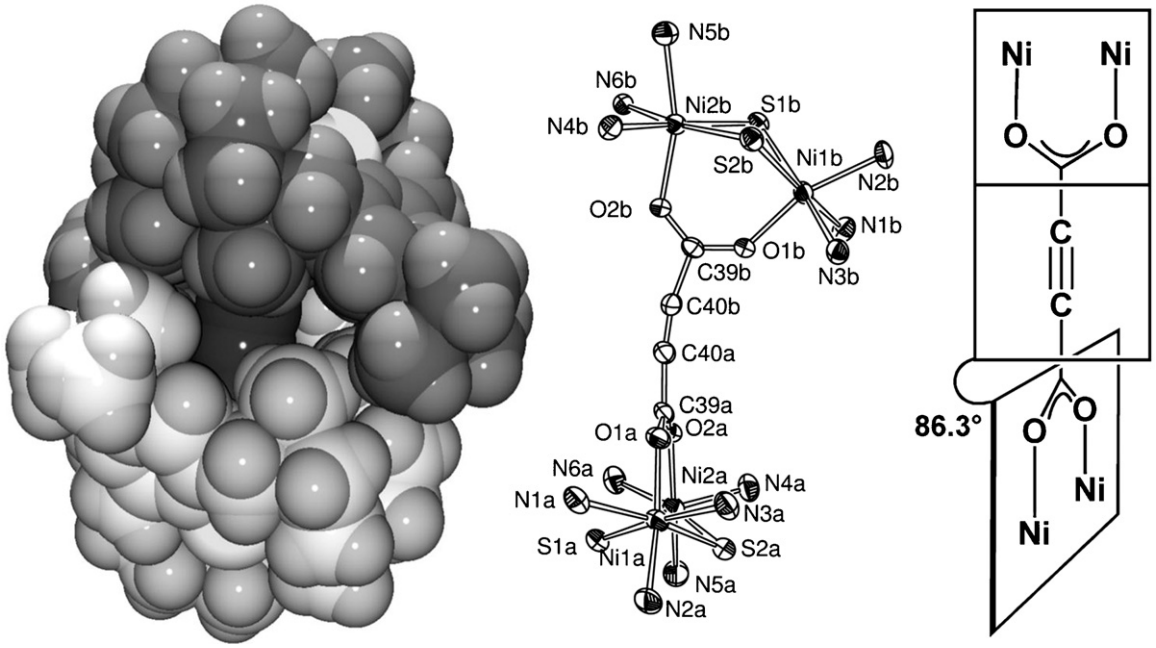

Fig. 17. (Left) Van der Waals plot of the structure of the $[\{Ni^{II}_2(L_6)\}_2(acetylenedicarboxylato)]^{2+}$ dication in crystals of **54**$[BPh_4]_2 \cdot MeCN \cdot 0.5H_2O$. Middle: ORTEP representation of the core structure of **54** with the atom labeling scheme. (Right) Mutual orientation of the Ni_2carboxylato planes in **54**. The figures were generated using data downloaded from The Cambridge Crystallographic Data Centre (CCDC) and correspond to the structure originally reported in Ref. [144].

3.5. Dinuclear complexes as building blocks for tetranuclear complexes

In view of the increasing interest in the targeted assembly of molecular-based magnetic materials using high-spin molecules of higher nuclearity [139–145], it was of interest to prepare tetranuclear complexes by linking pairs of dinuclear $[Ni^{II}_2(L^6)]$ entities via polydentate bridging ligands. Several such complexes were reported, and the ability of the bridging ligands to mediate long-range magnetic exchange interactions between the dinuclear subunits was examined.

The tetranuclear nickel(II) complexes $[\{Ni^{II}_2(L^6)\}_2$(acetylenedicarboxylate)$][BPh_4]_2$ (**54**$[BPh_4]_2$), $[\{Ni^{II}_2(L^6)\}_2$(terephthalate)$][BPh_4]_2$ (**55**$[BPh_4]_2$), $[\{Ni^{II}_2(L^6)\}_2$(isophthalate)$][BPh_4]_2$ (**56**$[BPh_4]_2$), and $[\{Ni^{II}_2(L^6)\}_2$(ferrocene-1,1′-dicarboxylate)$][BPh_4]_2$ (**57**$[BPh_4]_2$) have been synthesized by method a (see Section 3.4) and characterized by UV–vis spectroscopy, IR spectroscopy, and X-ray crystallography [107,146]. All dicarboxylates act as a quadridentate bridging ligands joining two bioctahedral $[Ni_2(L^6)]^{2+}$ units via $\mu_{1,3}$-bridging carboxylate functions to generate discrete $[\{Ni^{II}_2(L^6)\}_2(dicarboxylate)]^{2+}$ dications with a central $LNi_2(O_2C–R–CO_2)Ni_2L$ core (Fig. 17). The structures differ mainly in the distance between the center of the Ni···Ni axes of the isostructural $[Ni_2(L^6)]^{2+}$ units (8.841(1) Å in **54**, 10.712(1) Å in **55**, 9.561(1) Å in **56**, and 10.749 Å in **57**) and the tilting angle between the two Ni_2O_2 planes (86.3° in **54**, 58.2° in **55**, 20.9° in **56**, and 33.1° in **57**). Magnetic susceptibility measurements on the complexes over the temperature range 2.0–295 K reveal the presence of weak ferromagnetic exchange interactions between the Ni^{II} ions within the dinuclear subunits with values for the magnetic exchange constant J_1 of 23.1(5), 18.1(5), 14.2(5), and 22.0(5) cm^{-1} for **54**, **55**, **56**, and **57**, respectively ($H = -2JS_1S_2$). The magnitude of the exchange interaction J_2 across the dicarboxylate bridges is in all cases less than 0.1 cm^{-1}, suggesting that no significant interdimer exchange coupling occurs in **54**–**57**. A dependence of the *inter*dimer coupling on the mutual orientation of the Ni_2O_2 planes was not observed. High-spin molecules of this sort are presumably only accessible with shorter bridging ligands such as oxalate or squarate dianions.

The ability of the ligands 4,4′-bipyrazolyl (H_2L^{20}), 1,4-bis(4′-pyrazolyl)-benzene (H_2L^{21}), and 4,4′-bipyridazine (L^{22}) to link two dioctahedral $[Ni_2(L^6)]^{2+}$ units has also been examined [147]. The complexes $[Ni^{II}_2(L^6)(HL^{20})][BPh_4]$ (**58**$[BPh_4]$), $[Ni^{II}_2(L^6)(L^{22})][ClO_4]_2$ (**59**$[ClO_4]_2$), $[\{Ni^{II}_2(L^6)\}_2(bpzb)][BPh_4]_2$ (**60**$[BPh_4]_2$), and $[\{Ni^{II}_2(L^7)\}_2(bpz)][BPh_4]_2$ (**61**$[BPh_4]_2$) were

Table 4
Magnetic properties of some $[Ni_2(L^6)(L')]^+$ complexes

	L′	d(M···M) (Å)	M–S–M (°)	J (cm^{-1})	g	Refs.
10	$CH_3CO_2^-$	3.483(1)	89.65(4)	+6.4	2.25	[77,80]
29	OH^-	3.037(1)	76.95(4)	−6.60	2.20	[127]
38	BH_4^-	3.458(1)	89.41(5)	+27.0	2.09	[106]
40	O_2CPh^-	3.470(1)	89.09(4)	+5.8	2.20	[80]
42	NO_2^-	3.398(1)	87.03(4)	+6.7	2.26	[80]
43	N_3^-	3.683(1)	94.55(4)	−45.6	2.25	[80]
44	pydz	3.392(1)	87.58(2)	+3.5	2.38	[80]
47	SH^-	3.295(1)	83.31(3)	+18.0	2.23	[81]
49	SO_4^{2-}	3.506(1)	90.00(4)	+24.8	2.08	[105]
50	MoO_4^{2-}	n.d.		+2.35	2.17	[105]

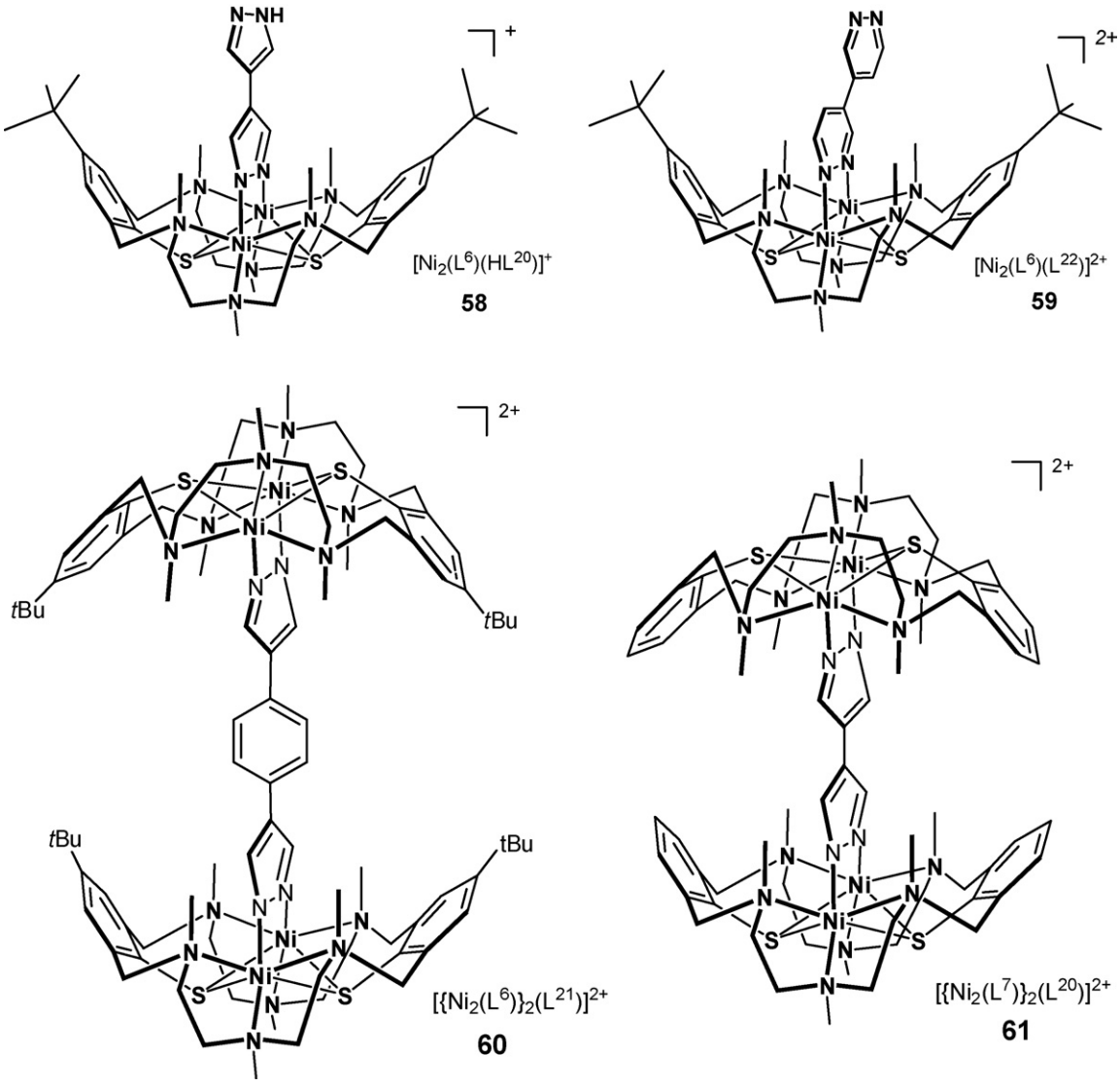

Fig. 18. Schematic representation of the structures of complexes **58**–**61** [145].

prepared (Fig. 18). Only the $(bpzb)^{2-}$ and $(bpz)^{2-}$ units act as tetradentate linkers. The $(Hbpz)^{-}$ and *bpdz* ligands in **58** and **59** act as bidentate ligands coordinating to only one $[Ni_2(L^6)]^{2+}$ unit.

The structures of the two tetranuclear complexes differ mainly in the distance between the center of the Ni···Ni axes of the isostructural $[Ni_2(L^6)]^{2+}$ and $[Ni_2(L^7)]^{2+}$ units (14.040(1) Å in **60**$[BPh_4]_2$, 9.184(1) Å in **61**$[BPh_4]_2$). The two Ni_2pyrazolato planes in **61**$[BPh_4]_2$ are coplanar. An analysis of the temperature-dependent magnetic susceptibility data for **61**$[BPh_4]_2$ reveals the presence of weak ferromagnetic exchange interactions between the Ni^{II} ions in the binuclear $[Ni_2(L^7)]^{2+}$ subunits with values for the magnetic exchange constant J_1 of 23.97 cm^{-1} ($H = -2JS_1S_2$). Again, the exchange coupling across the dipyrazolato bridge is less than 0.1 cm^{-1}, suggesting that no significant interdimer exchange coupling occurs in **61**$[BPh_4]_2$.

4. Electronic structure calculations

Recently, many experimental groups have devoted a considerable effort in the synthesis of new molecules presenting a long relaxation of the magnetization that can be considered like a single molecule magnet (SMM) [148]. In general the properties of such systems of coupled spins depend directly on the strength of the exchange coupling and of the spin–orbit coupling. When the exchange interactions are large enough, the lowest energy magnetic excitations in a many-spin system occur in fact due to collective changes in the spin–orbit coupling energy. The involved energy scale is known as the magnetic anisotropy energy [149]. The ability to accurately predict and modify the magnetic anisotropy energy is a key property one has to understand, because it determines the temperature range up to which a system will retain its magnetic orientation. Hence high magnetic anisotropy is one of major priorities in the design of useful molecular magnetic devices to apply them for the storage of information at the molecular (or nanoscale) level.

The height of the magnetic anisotropy barrier emerges by a quite subtle interplay between different factors, such as the exchange interaction that controls the total spin of the molecule, the strength of the spin–orbit coupling and the interaction with the crystal field due to the ligands. Thus, molecules with high total spin and large magnetic anisotropy are the targets in this field. However, there is no clear procedure available to design new systems with improved properties compared to known molecules. Therefore, the advances are to some extent due to serendipity. Hence, the application of

theoretical methods that can predict and help on the understanding of the two key factors, the exchange interactions and magnetic anisotropy, are crucial to help the experimentalist in the synthesis of new molecules with improved magnetic properties.

There has been a notable progress in the prediction of exchange interactions and magnetic anisotropy energies from density functional theory (DFT) [150] during the last few years. The calculation of exchange couplings seems nowadays possible and feasible even for larger systems using methods based on DFT. For recent reviews on the topic of calculation of exchange couplings by means of DFT, see, e.g., Ref. [151]. In contrast to cases where magnetic exchange interactions follow the famous Goodenough–Kanamori rules or the intuitive orbital dependence based on the Hay–Thibeault–Hoffmann or Kahn–Briatt models, we still have to await similarly clean general insights derived from theory in the case of magnetic anisotropy, which is another crucial property of molecular magnets. The ability to predict magnetic anisotropies reliable could revolutionize the rational design of molecular nanomagnets.

4.1. Theoretical background

To the best of our knowledge there has been so far only one theoretical study on the electronic and magnetic properties of a series of dinickel(II) complexes supported by the hexaaza-dithiophenolate ligand H_2L^6 [152] described in detail in the previous sections. This study was based on the Perdew–Burke–Ernzerhof (PBE) generalized-gradient approximation for the exchange and correlation functional [153] as implemented in the Gaussian-orbital-based program package NRLMOL [154].

The magnetic exchange coupling can be obtained using the broken symmetry approach. With help of the total energy differences between suitable selected ferromagnetic and antiferromagnetic spin configurations one can calculate the magnetic exchange constants J by mapping the energies to the same Heisenberg–Hamiltonian used for fitting the experimental data. Using a Hamiltonian of the form $H = -2JS_1S_2$ then a positive value for J would correspond to ferromagnetic (FM) and a negative one to antiferromagnetic (AFM) coupling, whereas S_1 and S_2 describe the spin operators of the different transition metal ions.

However, there is one conceptual problem following that route. Since DFT wavefunctions are only Eigenfunctions of the quantum spin operator S_z and not of the total S it is not possible to prepare proper AFM wavefunctions by means of DFT. For that reason the AFM state in DFT may be a combination of states with $m = 0$ belonging to different total S. Nevertheless, trends and sign of the magnetic exchange coupling are often in reasonable agreement with experiment. However, the value of J obtained from PBE is usually too large. This behavior seems to be a general failure of DFT since the standard DFT functionals do not localize the d-states strong enough as shown by Gunnarsson and Kortus [155].

There are several approaches to rationalize the magnetic coupling within a system of dinuclear transition metal complexes, the most often used is the application of the Goodenough–Kanamori rules [156]. These semi-empirical rules describe the strength and character of the magnetic coupling between two transition metal ions via a super-exchange mechanism across a bridging ligand. If there is an overlap of the magnetic orbitals of the bridging group and the magnetic orbitals of the transition metal ions, then one will find antiferromagnetic coupling. The larger this overlap gets, the stronger antiferromagnetic becomes the exchange. On the other hand ferromagnetic coupling is achieved if the overlap of the magnetic orbitals vanishes—this usually happens in case of a metal–bridge–metal angle of 90°.

Another, more quantitative approach is the Hay–Thibeault–Hoffmann (HTH) model [157]. The HTH-model describes weakly interacting metal centers in terms of configuration interaction of molecular orbitals. As shown in the original paper, for small interactions it becomes possible to relate the magnetic properties to the energies of the involved magnetic orbitals e_i at each metal center. In case of two nickel ions with d^8 configuration one can identify the two unoccupied d-orbitals at the nickel ions as the relevant magnetic orbitals. The difference Δe of squares of these orbital energies becomes a measure of the singlet-triplet energy splitting. A large Δe corresponds to strong antiferromagnetic coupling whereas a small value gives rise to ferromagnetic interaction.

The magnetic anisotropy D is calculated within NRLMOL by a perturbative approach proposed by Pederson [158], which relates the zero field splitting to spin orbit effects. A detailed discussion of the approach can be found in the literature [158].

4.2. Magnetic properties of $[M^{II}_2(L^6)(OAc)]^+$ complexes as a function of the metal ion M

First, we will focus on one selected coligand ($L' = OAc^-$) and discuss in detail the effect of varying the metal ion within the **3d** transition metal row, namely Co^{II}, Mn^{II}, Fe^{II} and Ni^{II}.

As shown in Table 6 one can observe ferromagnetic coupling only in case of Ni^{II}, all other metal complexes show an antiferromagnetic exchange interaction. Although the M···M distance is nearly the same there are large differences in the M^{II}–S–M^{II} angle. Here again the Goodenough–Kanamori rules can be used to give a good explanation for the observed magnetic coupling. In the case of Ni^{II} we find a M^{II}–S–M^{II} angle close to 90° leading consequently to ferromagnetic coupling. In case of smaller angles antiferromagnetic exchange pathways are opened, which will eventually dominate the ferromagnetic exchange contribution. Unfortunately, the Hay–Thibeault–Hoffmann model cannot be applied here, because it is limited to d^8 electron configuration only.

For the cases presented in Table 5 we find the usual overestimation of the values of J by DFT-based calculations. In the case of Co^{II} the situation is somewhat more complicated. A careful theoretical study of **3d** transition metal ions including a Co dimer using several exchange-correlation functionals including hybrid functionals found different ground state electronic configurations depending on the level of approximation [159]. Such situation may suggest the need for a multi reference description beyond the single determinant of DFT. Another complication arises due to the interaction of orbitally degenerate states, as is the case for low spin Co^{II} in an octahedral crystal field with one electron occupying the degenerated e_g-orbital. The Hamiltonian of the simple form $H = -2JS_1S_2$ is not correct anymore and additional interaction terms have to be considered [160], which makes the mapping of DFT obtained energies to a spin Hamiltonian of the above form not possible. For these reasons we do not provide any theoretical value for Co^{II} in Table 5. Overall we find reasonable good qualitative agreement between the exchange constants obtained from experiment and calculation. In particular the sign of the exchange coupling is in all cases reproduced correctly.

The variation of the transition metals allows only for limited changes of the magnetic properties. In contrast there is a large variety of coligands in case of nickel complexes, which makes it possible to tailor the magnetic exchange interaction. Therefore, we now focus our discussion on the effect of different coligands on the magnetic coupling and magnetic anisotropy in case of the $[Ni_2(L^6)(L')]^{n+}$ system.

Table 5
Magnetic properties and structural data of the $[M_2L^6(OAc)]^+$ complexes **10** and **23**–**25**

	M	J_{calcd} (cm^{-1})	J_{exp} (cm^{-1})	d(M^{II}–M^{II}) (Å)	M^{II}–S–M^{II} (°)	Refs.
10	Ni^{II}	33	6.4	3.483(1)	89.65(4)	[77]
23	Mn^{II}	−14	−5.05	3.456(1)	80.41(0)	[75]
24	Fe^{II}	−33	−10	3.421(1)	85.42(6)	[75]
25	Co^{II}		−1.9	3.448(1)	81.01(1)	[79]

4.3. Magnetic properties of $[Ni^{II}_2(L^6)(L')]$ complexes as a function of the bridging coligand L′

The series of the homodinuclear transition metal complexes $[M_2(L^6)(\mu\text{-}L')]^{n+}$ supported by the hexaazadithiopenolate ligand $(L^6)^{2-}$ is very interesting for systematic theoretical studies, because it allows to clarify the role and importance of the third bridging coligand (L′) with respect to the magnetic properties.

As shown in Table 6 and discussed before there exists an abundant selection of such bridging ligands L′—all of them belong to the conformational form of type B and differ in size and charge. Therefore one has to differentiate between structural and electronic effects influencing the magnetic exchange coupling between the nickel ions.

Nearly all of the complexes show ferromagnetic coupling with varying strength of the exchange coupling constant *J*. Only complexes **43** and **45** exhibit antiferromagnetic coupling of the Ni^{II} ions. In order to relate the magnetic properties to the structure of these complexes Table 5 also lists selected structural features, the $Ni^{II}\cdots Ni^{II}$ distances and the average Ni^{II}–S–Ni^{II} angle. The Ni^{II}–S–Ni^{II} angle of the azido complex **43** is considerably larger than 90° (Ni–S–Ni = 94.55°)—so one might expect antiferromagnetic behavior according to the Goodenough–Kanamori rules. On the other hand we find for complex **62** a similar deviation from the 90° angle (Ni^{II}–S–Ni^{II} angle = 86°). In both cases we find a deviation of about 4° from the 90° Ni^{II}–S–Ni^{II} angle, which would suggest antiferromagnetic coupling according to the Goodenough–Kanamori rules. However, complex **62** shows an overall ferromagnetic coupling. Therefore the coupling cannot be explained entirely by the Goodenough–Kanamori rules alone. Taking a closer look at the energy differences Δe defined by the Hay–Thibeault–Hoffmann model one can immediately see, that the largest Δe corresponds to the strongest antiferromagnetic coupling in complex **43**. This can be related to a strong interaction of the magnetic orbitals which is induced by the strong ligand field of the azido bridge. Also the somewhat longer Ni^{II}–Ni^{II} distance and the larger Ni^{II}–S–Ni^{II} angle add to this effect favoring antiferromagnetic coupling. In the case of **45** we also observe a relative large energy difference Δe compared to the cases which are coupled ferromagnetically. Nevertheless, the DFT calculations reveal only a small antiferromagnetic coupling. This can be explained due to the shorter Ni^{II}–Ni^{II} distance and the smaller deviation of Ni^{II}–S–Ni^{II} angle from 90°, leading to a larger ferromagnetic contribution compared with **43**.

A closer look at complex **44** shows, that Δe in that case has only half the value of complex **45**. At the same time the Ni^{II}–Ni^{II} distance and the Ni^{II}–S–Ni^{II} angle are in both cases nearly identical. This suggests that the effects on the electronic structure due to the chemical bonding of the third ligand become the deciding factor and somewhere between 0.06 $mRy^2 > \Delta e > 0.15$ mRy^2 the ferromagnetic interaction becomes favored.

If one compares the remaining energy differences they display all more or less similar values. Without the influence of additional structural effects one expects larger ferromagnetic coupling together with smaller values of Δe. However, there are some exceptions like for example complex **66**. Here one finds that the Ni^{II}–S–Ni^{II} angle is again close to 90°, which favors ferromagnetic coupling according to the Goodenough–Kanamori rules. Therefore structural changes and electronic effects can affect at the same time the magnetic coupling in this series of nickel complexes.

Table 6
Structural parameters, magnetic coupling *J*, magnetic anisotropy *D*, and the energy difference Δe of the Hay–Thibeault–Hoffmann model in $[Ni_2(L^6)(\mu\text{-}L')]^+$ complexes

Complex, Coligand	J_{calcd} (cm^{-1})	J_{exp} (cm^{-1})	D_{calcd} (cm^{-1})	D_{exp} (cm^{-1})	*d*(Ni–Ni) (Å)	Ni–S–Ni (°)	Δe (mRy^2)	Refs.
10, $CH_3CO_2^-$	33	6.4	0.20	|37.7|	3.483(1)	89.65(4)	0.0137	[77]
37, $CH_3OCO_2^-$	35	–	0.18	–	3.491(1)	90.00(6)	0.0066	[77]
38, BH_4^-	32	27	0.51	|4|	3.485(1)	89.41(5)	0.0241	[106]
39, $EtOCO_2^-$	37	–		–	3.485(1)	90.47(5)	0.0192	[77]
40, O_2CPh^-	31	5.8	0.33	−32	3.470(1)	89.09(4)	0.0085	[80]
41, NO_3^-	27	–	−0.32	–	3.492(1)	90.73(6)	0.0159	[80]
42, NO_2^-	25	6.7	0.47	−32	3.398(1)	87.03(4)	0.0473	[80]
43, N_3^-	−173	−45	0.99	0 (fix)	3.681(1)	94.55(4)	0.3131	[80]
44, *pydz*	11	3.5	0.65	9.53	3.392(1)	87.58(2)	0.0640	[80]
45, N_2H_4	−6	–	0.41	–	3.441(1)	87.74(3)	0.1453	[80]
46, HCO_2^-	27	–	0.17	–	3.480(1)	88.95(3)	0.0192	[106]
62, $C_3H_4N_2^-$,[a]	20	–	−0.34	–	3.388(1)	86.38(9)	0.0502	[80]
63, CO_2OH^-,[b]	26	–	−0.47	–	3.471(1)	89.25(8)	0.0433	[80]
64, $C_5H_8CO_2^-$,[c]	33	–	0.18	–	3.472(1)	89.46(9)	0.0103	[62]
65, $HO(CH_2)_2OCO_2^-$,[d]	34	–	−0.14	–	3.490(1)	89.89(4)	0.0490	[77]
66, *m*-Cl-$C_6H_4CO_2^-$,[e]	35	–	0.19	–	3.460(1)	89.95(12)	0.076	[88]
67, $C_{15}H_{17}O_2^-$,[f]	35	–	0.28	–	3.486(1)	90.12(12)	0.0151	[62]
68, $C_8H_6N_2$,[g]	22	–	−0.44	–	3.402(1)	88.06(4)	0.0307	[80]

[a] $\mu_{1,2}$-Pyrazolato.
[b] $\mu_{1,3}$-Bicarbonato.
[c] $\mu_{1,3}$-(2*E*,4*E*)-Hexa-2,4-dienoate.
[d] $\mu_{1,3}$-2-(Hydroxyethyl)Carbonato.
[e] $\mu_{1,3}$-*meta*-Chlorobenzoato.
[f] $\mu_{1,3}$-3,4-Dimethyl-6-phenylcyclohex-3-ene-1-carboxylato.
[g] $\mu_{1,2}$-Phthalazine.

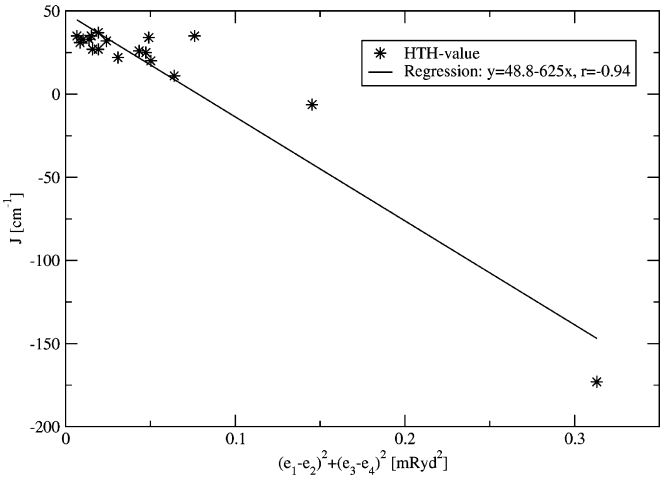

Fig. 19. Plot of Δe against J_{calcd} for $[Ni_2(L^6)(L')]^{n+}$ complexes including a linear least-squares fit according to the Hay–Thibeault–Hoffmann (HTH) model [155].

The discussed relation between the values of Δe and the calculated magnetic exchange constant J_{calcd} is presented in Fig. 19. Due to small differences in local structural environment of the magnetic nickel dimer core in the investigated complexes the data deviates from a perfect linear dependency. A least-squares fit of the data predicts a maximal possible ferromagnetic J value of about 50 cm^{-1}. This suggests, that this family of nickel amine-thiophenolate complexes is limited to that maximal value of ferromagnetic coupling regardless of other possible coligands L′.

As shown by Loose and co-workers [152] the bridging ligand L′ in $[Ni^{II}_2(L^6)(L')]^{n+}$ complexes plays a crucial role in the type and magnitude of the magnetic coupling. In some cases the bridge provides the largest contribution to the ferromagnetic coupling. Fig. 20 shows a plot of a molecular orbital presenting a distinctive pathway across the $\mu_{1,3}$-BH_4 ion of complex **38**.

As one can see, this exchange pathway across the bridge involves d-orbitals at the Ni^{II} centers and a p-orbital from the bridging BH_4^- ion. Similar behavior can be observed for all investigated models except **43** and **45**. However, it is most pronounced in complex **38**. In the case of **43**, the N_3^- coligand changes the orbital energies

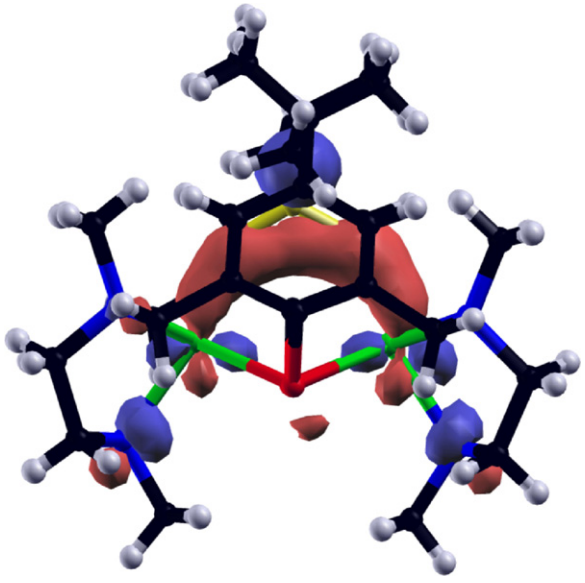

Fig. 20. Exchange pathway across the bridge of complex **38** [150].

in such a way, that the ferromagnetic exchange pathway across the coligand becomes blocked. This is not surprising, since N_3^- is known as a ligand inducing a strong ligand field. In order to tune the magnetic coupling to higher ferromagnetic couplings one should investigate weak coligands, since they may provide an additional ferromagnetic pathway without inducing a further increase of the singlet–triplet splitting. At the same time the coligand should have the appropriate geometrical size in order to keep the general structure of type B.

While it appears possible to rationalize the observed magnetic exchange properties in terms of structural and electronic elements, the situation changes completely in case of magnetic anisotropy D. A single molecule magnet can be defined by a negative D, because in that case the magnetization orients itself along a preferred axis, which results in a barrier for reversal of the direction of the magnetization. The blocking temperature up to which a magnetic system retains its magnetization is directly related to the value of D.

Table 6 summarizes the calculated magnetic anisotropy parameters D. There are several effects involving the determination of D. One important feature of the coligand is its ligand field strength. As shown in the literature [152] a strong ligand field leads to a small value of D. On the other hand the octahedral environment of the Ni^{II} ions will be important, because magnetic anisotropy vanishes in case of cubic symmetry. The larger the deviation from the perfect octahedron, the larger the magnetic anisotropy. The most favorable case would be a molecule with a large spin ground state S and a large negative magnetic anisotropy parameter D, because the barrier height is calculated as $S^2|D|$. At first glance this seems to imply, that it is more effective to raise the spin ground state than trying to increase the magnetic anisotropy. However, this might not be true. As recently shown [161] the simple approach is not sufficient due to an intrinsic dependence of the magnetic anisotropy on the spin state. In fact, a large magnetic anisotropy and a large spin ground state seem not to be favored at the same time [162].

5. Concluding remarks

The development, synthesis, and the coordination chemistry of novel macrobinucleating amine-thiophenolate ligands has been described. It was demonstrated that the doubly deprotonated forms of the macrocycles $(L^R)^{2-}$ support the formation of mixed-ligand complexes of the type $[M_2(L^R)(\mu\text{-}L')]$ with either a face sharing or edge sharing bioctahedral $N_3M(\mu\text{-}S)_2(\mu\text{-}L')MN_3$ core structure. Despite the fact that the active coordination site L′ is deeply buried, it is readily accessible for a wide range of exogenous guest molecules. A large number of crystal structure determinations have provided insights into the binding modes of the coligands. These sense the size and form of the binding pocket of the $[M_2(L^R)]^{2+}$ fragments as indicated by distinctive binding modes and unusual conformations. The use of the N-alkylated macrocycles in place of the unmodified analogs influences many properties of the binuclear complexes, including color, molecular and electronic structure, hydrogen bonding interactions, redox potential, complex stability, and ground spin-state.

Electronic structure calculations are a very powerful tool to elucidate the interplay between structural and electronic changes by theoretical means. The DFT calculations for a set of dinuclear nickel(II) complexes reveal that the exogenous coligand is very important for the sign and value of the exchange coupling constant, not only due to a change in geometry but also due to electronic effects. The bridge determines the sign and value of the magnetic interaction by opening new exchange pathways through the bridge. This possibility opens an interesting avenue to tune the sign and size of the magnetic interaction by choosing

an appropriate bridge. The experimental observed behavior (better "magnetic properties") can be well understood in terms of the Hay–Thibeault–Hoffmann model, while the magnetic anisotropy parameters relates to the crystal field strength of the third bridging ligand and the deviation of the local Ni environment from a perfect octahedron.

Acknowledgements

Several co-workers named on our joint publications have made major contributions to the chemistry described in this article. Without their dedication and ingenuity, this chemistry would not have reached its current level of broad synthetic utility. B.K. is thankful for Prof. H. Vahrenkamp and Prof. Dr. H. Krautscheid for providing facilities for spectroscopic and X-ray crystallographic measurements. This work was supported by the Deutsche Forschungsgemeinschaft (Projects KE 585/4-1,2,3), the University of Freiburg, and the University of Leipzig. C.L. and J.K. would like to thank the German DAAD and the DFG for financial support within the priority programme "SPP 1137, Molecular Magnetism". The authors thankfully acknowledge the computer resources, technical expertise and assistance provided by ZIH TU Dresden.

References

[1] I.G. Dance, Polyhedron 5 (1986) 1037.
[2] B. Krebs, G. Henkel, Angew. Chem. 105 (1991) 785;
B. Krebs, G. Henkel, Angew. Chem., Int. Ed. Engl. 30 (1991) 769.
[3] J. Arnold, Prog. Inorg. Chem. 43 (1995) 353.
[4] P.J. Blower, J.R. Dilworth, Coord. Chem. Rev. 76 (1987) 121.
[5] M.A. Halcrow, G. Christou, Chem. Rev. 94 (1994) 2421.
[6] G. Henkel, B. Krebs, Chem. Rev. 104 (2004) 801.
[7] A.C. Marr, D.J.E. Spencer, M. Schröder, Coord. Chem. Rev. 219–221 (2001) 1055.
[8] T.C. Harrop, P.K Mascharak, in: H.-B. Kraatz, N. Metzler-Nolte (Eds.), Concepts and Models in Bioinorganic Chemistry, 1st ed., Wiley–VCH, 2006, p. 309.
[9] D. Sellmann, J. Sutter, Acc. Chem. Res. 30 (1997) 460.
[10] C.A. Grapperhaus, M.J. Darensbourg, Acc. Chem. Res. 31 (1998) 451.
[11] T. Beissel, K.S. Bürger, G. Voigt, K. Wieghardt, C. Butzlaff, A.X. Trautwein, Inorg. Chem. 32 (1993) 124.
[12] T. Glaser, T. Beissel, E. Bill, T. Weyhermüller, V. Schünemann, W. Meyer-Klaucke, A.X. Trautwein, K. Wieghardt, J. Am. Chem. Soc. 121 (1999) 2193.
[13] H.-J. Krüger, R.H. Holm, J. Am. Chem. Soc. 112 (1990) 2955.
[14] P. Zanello, S. Tamburini, P.A. Vigato, G.A. Mazzochin, Coord. Chem. Rev. 77 (1987) 165.
[15] N. Sträter, W.N. Lipscomb, T. Klabunde, B. Krebs, Angew. Chem. 108 (1996) 2158;
N. Sträter, W.N. Lipscomb, T. Klabunde, B. Krebs, Angew. Chem., Int. Ed. 35 (1996) 2024.
[16] D.G. Mccollum, G.P.A. Yap, A.L. Rheingold, B. Bosnich, J. Am. Chem. Soc. 118 (1996) 1365.
[17] A.L. Gavrilova, C.J. Qin, R.D. Sommer, A.L. Rheingold, B. Bosnich, J. Am. Chem. Soc. 124 (2002) 1714.
[18] S. Brooker, Coord. Chem. Rev. 222 (2001) 33.
[19] N.H. Pilkington, R. Robson, Aust. J. Chem. 23 (1970) 2225.
[20] D.E. Fenton, P.A. Vigato, Chem. Soc. Rev. 17 (1988) 69.
[21] P.A. Vigato, S. Tamburini, D. Fenton, Coord. Chem. Rev. 106 (1990) 25.
[22] D. Fenton, Chem. Soc. Rev. 28 (1999) 159.
[23] H. Okawa, H. Furutachi, D.E. Fenton, Coord. Chem. Rev. 174 (1998) 51.
[24] A.J. Atkins, D. Black, A.J. Blake, A. Marin-Becerra, S. Parsons, L. Ruiz-Ramirez, M. Schröder, Chem. Commun. (1996) 457.
[25] N.E. Borisova, M.D. Reshetova, Y.A. Ustynyuk, Chem. Rev. 107 (2007) 46.
[26] For biological, dithiolate-bridged Cu/Cu systems, see;
(a) T. Tsukihara, H. Aoyama, E. Yamashita, T. Tomizaki, H. Yamaguchi, K. Shinzawa-Itoh, R. Nakashima, R. Yaono, S. Yoshikawa, Science 269 (1995) 1069;
(b) S. Iwata, C. Ostermeier, B. Ludwig, H. Michel, Nature 376 (1995) 660;
(c) M. Wilmanns, P. Lappalainen, M. Kelly, E. Saver-Eriksson, M. Saraste, Proc. Natl. Acad. Sci. U.S.A. 92 (1995) 11949.
[27] For biological, dithiolate-bridged Fe/Ni systems, see:
(a) A. Volbeda, M.-H. Charon, C. Piras, E.C. Hatchikian, M. Frey, J.C. Fontecilla-Camps, Nature 376 (1995) 660;
(b) A. Volbeda, E. Garcin, C. Piras, A.L. de Lacey, V.M. Fernandez, E.C. Hatchikian, M. Frey, J.C. Fontecilla-Camps, J. Am. Chem. Soc. 118 (1996) 12989;
(c) M.A. Halcrow, Angew. Chem. 107 (1995) 1307;
(d) M.A. Halcrow, Angew. Chem., Int. Ed. Engl. 34 (1995) 1193.
[28] For biological, dithiolate-bridged Fe/Fe systems, see:
(a) J.W. Peters, W.N. Lanzilotta, B.J. Lemon, L.C. Seefeldt, Science 282 (1998) 1853;
(b) R. Cammack, Adv. Inorg. Chem. 38 (1992) 281.
[29] G.A. Lawrance, M. Maeder, T.M. Manning, M.A. O'Leary, B.W. Skelton, A.H. White, J. Chem. Soc., Dalton Trans. (1990) 2491.
[30] A.J. Atkins, A.J. Blake, M. Schröder, J. Chem. Soc., Chem. Commun. (1993) 1662.
[31] S. Brooker, P.D. Croucher, F.M. Roxburgh, J. Chem. Soc., Dalton Trans. (1996) 3031.
[32] S. Brooker, P.D. Croucher, J. Chem. Soc., Chem. Commun. (1995) 1493.
[33] S. Brooker, P.D. Croucher, J. Chem. Soc., Chem. Commun. (1995) 2075.
[34] S. Brooker, P.D. Croucher, Chem. Commun. (1997) 459.
[35] S. Brooker, T.C. Davidson, Chem. Commun. (1997) 2007.
[36] S. Brooker, P.D. Croucher, T.C. Davidson, G.S. Dunbar, A.J. McQuillan, G.B. Jameson, Chem. Commun. (1998) 2131.
[37] S. Brooker, G.B. Caygill, P.D. Croucher, T.C. Davidson, D.L.J. Clive, S.R. Magnuson, S.P. Cramer, C.Y. Raston, J. Chem. Soc., Dalton Trans. (2000) 3113.
[38] S. Brooker, P.D. Croucher, T.C. Davidson, G.S. Dunbar, C.U. Beck, S. Subramanian, Eur. J. Inorg. Chem. (2000) 169.
[39] A. Christensen, H.S. Jensen, V. McKee, C.J. McKenzie, M. Munch, Inorg. Chem. 36 (1997) 6080.
[40] P.E. Kruger, V. McKee, Chem. Commun. (1997) 1341.
[41] N.D.J. Branscombe, A.J. Blake, A. Marin-Becerra, W.S. Li, S. Parsons, L. Ruiz-Ramirez, M. Schröder, Chem. Commun. (1996) 2573.
[42] N.D.J. Branscombe, A.J. Atkins, A. Marin-Becerra, E.J.L. McInnes, F.E. Mabbs, J. McMaster, M. Schröder, Chem. Commun. (2003) 1098.
[43] P.A. Vigato, S. Tamburini, L. Bertolo, Coord. Chem. Rev. 251 (2007) 1311.
[44] M.P. Suh, in: A.G. Sykesed (Ed.), Advanced Inorg. Chem., Vol. 44, Academic Press, New York, 1997, p. 93.
[45] E.C. Constable, Metals and Ligand Reactivity, VCH, Weinheim, 1996.
[46] H. Adams, N.A. Bailey, D.E. Fenton, R.J. Good, R. Moody, C.O.R. de Barbarin, J. Chem. Soc., Dalton Trans. (1987) 207.
[47] C.J. Harding, Q. Lu, J.F. Malone, D.J. Marrs, N. Martin, V. McKee, J. Nelson, J. Chem. Soc., Dalton Trans. (1995) 1739.
[48] S. Brooker, V. McKee, Inorg. Chim. Acta 173 (1990) 69.
[49] M.H. Klingele, G. Steinfeld, B. Kersting, Z. Naturforsch. 56b (2001) 901.
[50] M.H. Klingele, B. Kersting, Z. Naturforsch. 56b (2001) 437.
[51] G. Illuminati, L. Mandolini, Acc. Chem. Res. 14 (1981) 95.
[52] F. Diederich, P.J. Stang (Eds.), Templated Organic Synthesis, Wiley–VCH, Weinheim, 2000.
[53] D.H. Busch, N.A. Stephenson, Coord. Chem. Rev. 100 (1990) 119.
[54] B. Kersting, G. Steinfeld, T. Fritz, J. Hausmann, Eur. J. Inorg. Chem. (1999) 2167.
[55] B. Kersting, Z. Naturforsch. 55b (2000) 961.
[56] B. Kersting, G. Steinfeld, Chem. Commun. (2001) 1376.
[57] M. Gressenbuch, V. Lozan, G. Steinfeld, B. Kersting, Eur. J. Inorg. Chem. (2005) 2223.
[58] M. Gressenbuch, B. Kersting, Eur. J. Inorg. Chem. (2007) 90.
[59] T. Gregor, C.F. Weise, V. Lozan, B. Kersting, Synthesis (2007) 3706.
[60] V. Lozan, B. Kersting, Z. Anorg. Allg. Chem. 634 (2008) 941.
[61] M. Gressenbuch, PhD Thesis, University of Leipzig, Germany, 2008.
[62] S. Käss, T. Gregor, B. Kersting, Angew. Chem. 118 (2006) 107;
S. Käss, T. Gregor, B. Kersting, Angew. Chem., Int. Ed. 45 (2006) 101.
[63] G. Siedle, B. Kersting, Z. Anorg. Allg. Chem. 629 (2003) 2083.
[64] C.D. Gutsche, Calixarenes, Royal Society of Chemistry, Cambridge, UK, 1989.
[65] R.R. Gagne, C.L. Spiro, T.J. Smith, C.A. Hamann, W.R. Thies, A.K. Shiemke, J. Am. Chem. Soc. 103 (1981) 4073.
[66] S.L. Lambert, C.L. Spiro, R.R. Gagne, D.N. Hendrickson, Inorg. Chem. 21 (1982) 68.
[67] D.G. McCollum, G.P.A. Yap, A.L. Rheingold, B. Bosnich, J. Am. Chem. Soc. 118 (1996) 1365.
[68] H. Okawa, J. Nishio, M. Ohba, M. Tadokoro, N. Matsumoto, M. Koikawa, S. Kida, D.E. Fenton, Inorg. Chem. 32 (1993) 2949.
[69] M. Yamami, H. Furutachi, T. Ykoyama, H. Okawa, Inorg. Chem. 37 (1998) 6832.
[70] M. Yonemura, Y. Matsumura, H. Furutachi, M. Ohba, H. Okawa, D.E. Fenton, Inorg. Chem. 36 (1997) 2711.
[71] H. He, A.E. Martell, R.J. Motekaitis, J.H. Reibenspies, Inorg. Chem. 39 (2000) 1586.
[72] J. Nishio, H. Okawa, S. Ohtsuka, M. Tomono, Inorg. Chim. Acta 218 (1994) 27.
[73] T. Fritz, G. Steinfeld, S. Käss, B. Kersting, Dalton Trans. (2006) 3812.
[74] A.W. Addison, T.N. Rao, J. Reedijk, J. Van Rijn, G.C. Verschoor, J. Chem. Soc., Dalton Trans. (1984) 1349.
[75] Y. Journaux, T. Glaser, G. Steinfeld, V. Lozan, B. Kersting, Dalton Trans. (2006) 1738.
[76] A. Christensen, C. Mayer, F. Jensen, A.D. Bond, C.J. McKenzie, Dalton Trans. (2006) 108.
[77] B. Kersting, Angew. Chem. 113 (2001) 4110;
B. Kersting, Angew. Chem., Int. Ed. 40 (2001) 3988.
[78] V. Lozan, B. Kersting, Eur. J. Inorg. Chem. (2005) 504.
[79] B. Kersting, G. Steinfeld, Inorg. Chem. 41 (2002) 1140.
[80] J. Hausmann, M.-H. Klingele, V. Lozan, G. Steinfeld, D. Siebert, Y. Journaux, J.-J. Girerd, B. Kersting, Chem. Eur. J. 10 (2004) 1716.
[81] V. Lozan, B. Kersting, Inorg. Chem. 47 (2008) 5386.
[82] D. Kong, A.E. Martell, R.J. Motekaitis, J.H. Reibenspies, Inorg. Chim. Acta 317 (2001) 243.
[83] J. Wang, A.E. Martell, J.H. Reibenspies, Inorg. Chim. Acta 328 (2002) 53.

[84] D. Kong, A.E. Martell, J.H. Reibenspies, Inorg. Chim. Acta 333 (2002) 7.
[85] J. Gao, A.E. Martell, J. Reibenspies, Inorg. Chim. Acta 346 (2003) 32.
[86] J. Gao, A.E. Martell, J. Reibenspies, Inorg. Chim. Acta 329 (2002) 122.
[87] N.N. Greenwood, A. Earnshaw, Chemistry of the Elements, VCH, Weinheim, 1988.
[88] J. Hausmann, S. Käss, B. Kersting, S. Klod, E. Kleinpeter, Eur. J. Inorg. Chem. (2004) 4402.
[89] G. Steinfeld, PhD Thesis, University of Freiburg, Germany, 2004.
[90] J.C. Fontecilla-Camps, A. Volbeda, C. Cavazza, Y. Nicolet, Chem. Rev. 107 (2007) 4273.
[91] T.I. Doukov, T.M. Iverson, J. Seravalli, S.W. Ragsdale, C.L. Drennan, Science 298 (2002) 567.
[92] X. Liu, S.K. Ibrahim, C. Tard, C.J. Pickett, Coord. Chem. Rev. 249 (2005) 1641.
[93] E. Bouwman, J. Reedijk, Coord. Chem. Rev. 249 (2005) 1555.
[94] C. Mealli, T.B. Rauchfuss, Angew. Chem. 119 (2007) 9100;
C. Mealli, T.B. Rauchfuss, Angew. Chem., Int. Ed. 46 (2007) 8942.
[95] B. Kersting, D. Siebert, D. Volkmer, M.J. Kolm, C. Janiak, Inorg. Chem. 38 (1999) 3871.
[96] B. Kersting, D. Siebert, Inorg. Chem. 37 (1998) 3820.
[97] B. Kersting, D. Siebert, Eur. J. Inorg. Chem. (1999) 189.
[98] G. Steinfeld, B. Kersting, Chem. Commun. (2000) 205.
[99] E.K. Barefield, G.M. Freeman, D.G. Van Derveer, Inorg. Chem. 25 (1986) 552.
[100] F.A. Cotton, G. Wilkinson, C.A. Murillo, M. Bochman, Advanced Inorganic Chemistry, 6th ed., Wiley-Interscience, New York, 1999, p. 838.
[101] A.B.P. Lever, Inorganic Electronic Spectroscopy, 2nd ed., Elsevier Science, Amsterdam, 1984.
[102] T. Beissel, T. Glaser, F. Kesting, K. Wieghardt, B. Nuber, Inorg. Chem. 35 (1996) 3936.
[103] V. Lozan, B. Kersting, Inorg. Chem. 45 (2006) 5630.
[104] G. Steinfeld, V. Lozan, B. Kersting, Angew. Chem. 115 (2003) 2363;
G. Steinfeld, V. Lozan, B. Kersting, Angew. Chem., Int. Ed. 42 (2003) 2261.
[105] V. Lozan, B. Kersting, Eur. J. Inorg. Chem. (2007) 1436.
[106] Y. Journaux, J. Hausmann, V. Lozan, B. Kersting, Chem. Commun. (2006) 83.
[107] V. Lozan, A. Buchholz, W. Plass, B. Kersting, Chem. Eur. J. 13 (2007) 7305.
[108] V. Lozan, J. Holldorf, B. Kersting, Inorg. Chim. Acta, in press, doi:10.1016/j.ica.2008.03.016.
[109] V. Lozan, S.V. Votekovich, P.N. Gaponik, O.A. Ivashkevich, B. Kersting, Z. Naturforsch. 63b (2008) 496.
[110] C.G. Pierpont, D.N. Hendrickson, D.M. Duggan, F. Wagner, E.K. Barefield, Inorg. Chem. 14 (1975) 604.
[111] P. Chaudhuri, M. Guttmann, D. Ventur, K. Wieghardt, B. Nuber, J. Weiss, J. Chem. Soc., Chem. Commun. (1985) 1618.
[112] J. Ribas, A. Escuer, M. Monfort, R. Vicente, R. Cortes, L. Lezama, T. Rojo, Coord. Chem. Rev. 193–195 (1999) 1027.
[113] C.J. Harding, F.E. Mabbs, E.J. MacInnes, V. McKee, J. Nelson, J. Chem. Soc., Dalton Trans. (1996) 3227.
[114] A. Escuer, C.J. Harding, Y. Dussart, J. Nelson, V. McKee, R. Vicente, J. Chem. Soc., Dalton Trans. (1999) 223.
[115] A. Escuer, R. Vicente, J. Ribas, M.S. El Fallah, X. Solans, M. Font-Bardia, Inorg. Chem. 32 (1993) 3727.
[116] A. Escuer, R. Vicente, J. Ribas, M.S. El Fallah, X. Solans, M. Font-Bardia, Inorg. Chem. 33 (1994) 1842.
[117] A.F. Hollemann, E. Wiberg, Lehrbuch der Anorganischen Chemie, Vol. 91, Walter de Gruyter, Berlin, 1985 (100 ed, p. 557).
[118] D. Sellmann, H. Kunstmann, F. Knoch, M. Moll, Inorg. Chem. 27 (27) (1988) 4183.
[119] D. Sellmann, W. Soglowek, F. Knoch, M. Moll, Angew. Chem. 101 (1989) 1244;
D. Sellmann, W. Soglowek, F. Knoch, M. Moll, Angew. Chem., Int. Ed. Engl. 28 (1989) 1271.
[120] R.A. Henderson, G.J. Leigh, C.J. Pickett, Adv. Inorg. Chem. Radiochem. 27 (1983) 197.
[121] D. Sutton, Chem. Rev. 93 (1993) 995.
[122] D. Sellmann, K. Engl, F.W. Heinemann, J. Sieler, Eur. J. Inorg. Chem. (2000) 1079.
[123] K. Matsumoto, T. Koyama, Y. Koide, J. Am. Chem. Soc. 121 (1999) 10913.
[124] S. Matsukawa, S. Kuwata, Y. Ishii, M. Hidai, J. Chem. Soc., Dalton Trans. (2002) 2737.
[125] L. Blum, I.D. Williams, R.R. Schrock, J. Am. Chem. Soc. 106 (1984) 8316.
[126] R.C. Murray, R.R. Schrock, J. Am. Chem Soc. 107 (1985) 4557.
[127] V. Lozan, B. Kersting, unpublished results.
[128] A.P. Ginsberg, Inorg. Chim. Acta Rev. 5 (1971) 45.
[129] O. Kahn, Molecular Magnetism, VCH, Weinheim, 1993.
[130] T. Beissel, F. Birkelbach, E. Bill, T. Glaser, F. Kesting, C. Krebs, T. Weyhermüller, K. Wieghardt, C. Butzlaff, A.X. Trautwein, J. Am. Chem. Soc. 118 (1996) 12376.
[131] U. Bossek, D. Nühlen, E. Bill, T. Glaser, C. Krebs, T. Weyhermüller, K. Wieghardt, M. Lengen, A.X. Trautwein, Inorg. Chem. 36 (1997) 2834.
[132] Y. Elerman, M. Kabak, I. Svoboda, H. Fuess, K. Griesar, W. Haase, Z. Naturforsch. 51b (1996) 1132.
[133] J. Ribas, M. Montfort, I. Resino, X. Solans, P. Rabu, F. Maingot, M. Drillon, Angew. Chem. 108 (1996) 2671;
J. Ribas, M. Montfort, I. Resino, X. Solans, P. Rabu, F. Maingot, M. Drillon, Angew. Chem., Int. Ed. Engl. 35 (1996) 2520.
[134] A. Escuer, R. Vicente, J. Ribas, M.S. El Fallah, X. Solans, M. Font-Bardía, Inorg. Chem. 32 (1993) 3727.
[135] A. Escuer, R. Vicente, J. Ribas, M.S. El Fallah, X. Solans, M. Font-Bardía, Inorg. Chem. 33 (1994) 1842.
[136] A. Escuer, R. Vicente, M.S. El Fallah, J. Ribas, X. Solans, M. Font-Bardía, J. Chem. Soc., Dalton Trans. (1993) 2975.
[137] R. Vicente, A. Escuer, J. Ribas, M.S. El Fallah, X. Solans, M. Font-Bardía, Inorg. Chem. 34 (1995) 1278.
[138] J. Ribas, M. Montfort, B.K. Ghosh, R. Cortés, X. Solans, M. Font-Bardía, Inorg. Chem. 35 (1996) 864.
[139] J.S. Miller, M. Drillon (Eds.), Magnetism: Molecules to Materials, Wiley–VCH, Weinheim, 2001.
[140] E. Coronado, P. Delhaes, D. Gatteschi, J.S. Miller (Eds.), Molecular Magnetism: From Molecular Assemblies to Devices, NATO ASI Series, Kluwer, Dordrecht, The Netherlands, 1995, p. 321.
[141] S.P. Watton, P. Fuhrmann, L.E. Pence, A. Caneschi, A. Cornia, G.L. Abbati, S.J. Lippard, Angew. Chem. 109 (1997) 2917;
S.P. Watton, P. Fuhrmann, L.E. Pence, A. Caneschi, A. Cornia, G.L. Abbati, S.J. Lippard, Angew. Chem., Int. Ed. Engl. 36 (1997) 2774.
[142] J. Larionova, M. Gross, M. Pilkington, H. Andres, H. Stoeckli-Evans, H.U. Güdel, S. Decurtins, Angew. Chem. 112 (2000) 1667;
J. Larionova, M. Gross, M. Pilkington, H. Andres, H. Stoeckli-Evans, H.U. Güdel, S. Decurtins, Angew. Chem., Int. Ed. 39 (2000) 1605.
[143] A.L. Dearden, S. Parsons, R.E.P. Winpenny, Angew. Chem. 113 (2001) 155;
A.L. Dearden, S. Parsons, R.E.P. Winpenny, Angew. Chem., Int. Ed. 40 (2001) 151.
[144] S. Demeshko, G. Leibeling, S. Dechert, F. Meyer, Dalton Trans. (2006) 3458.
[145] B. Kersting, G. Steinfeld, D. Siebert, Chem. Eur. J. 7 (2001) 4253.
[146] J. Hausmann, M.H. Klingele, O. Baars, V. Lozan, A. Buchholz, G. Leibeling, W. Plass, F. Meyer, B. Kersting, Eur. J. Inorg. Chem. (2007) 5277.
[147] V. Lozan, P.Y. Solntsev, G. Leibeling, K.V. Domasevitch, B. Kersting, Eur. J. Inorg. Chem. (2007) 3217.
[148] D. Gatteschi, R. Sessoli, Angew. Chem. 115 (2003) 278;
D. Gatteschi, R. Sessoli, Angew. Chem., Int. Ed. 42 (2003) 268.
[149] J. van Vleck, Phys. Rev. 52 (1937) 1178.
[150] (a) P. Hohenberg, W. Kohn, Phys. Rev. 136 (1964) B864;
(b) W. Kohn, L.J. Sham, Phys. Rev. 140 (1965) A1133.
[151] E. Ruiz, Struct. Bonding 113 (2004) 71.
[152] C. Loose, E. Ruiz, B. Kersting, J. Kortus, Chem. Phys. Lett. 452 (2008) 38.
[153] J.P. Perdew, K. Burke, M. Ernzerhof, Phys. Rev. Lett. 77 (1996) 3865.
[154] (a) M.R. Pederson, K.A. Jackson, Phys. Rev. B 41 (1990) 7453;
(b) K.A. Jackson, M.R. Pederson, Phys. Rev. B 42 (1990) 3276.
[155] (a) O. Gunnnarsson, B.I. Lundqvist, Phys. Rev. B 13 (1976) 4274;
(b) J. Kortus, C.S. Hellberg, M.R. Pederson, Phys. Rev. Lett. 86 (2001) 3400.
[156] (a) J.B. Goodenough, Phys. Rev. 100 (1955) 564;
(b) J.B. Goodenough, Phys. Chem. Solids 6 (1958) 287;
(c) J. Kanamori, Phys. Chem. Solids 10 (1959) 87.
[157] P.J. Hay, J.C. Thibeault, R. Hoffmann, J. Am. Chem. Soc. 97 (1975) 4884.
[158] (a) M.R. Pederson, S.N. Khanna, Phys. Rev. B 60 (1999) 9566;
(b) J. Kortus, M.R. Pederson, T. Baruah, N. Bernstein, C.S. Hellberg, Polyhedron 22 (2003) 1871;
(c) A.V. Postnikov, J. Kortus, M.R. Pederson, Phys. Status Solidi B 243 (2006) 2533;
(d) J. Ribas-Arino, T. Baruah, M.R. Pederson, J. Am. Chem. Soc. 128 (2006) 9497.
[159] C.J. Barden, J.C. Rienstra-Kiracofe, H.F. Schaefer III, J. Chem. Phys. 113 (2000) 690.
[160] M. Drillon, R. Georges, Phys. Rev. B 24 (1981) 1278.
[161] O. Waldmann, Inorg. Chem. 46 (2007) 10035.
[162] E. Ruiz, J. Cirera, J. Cano, S. Alvarez, C. Loose, J. Kortus, Chem. Commun. (2008) 52.